nature climate change

LETTERS

https://doi.org/10.1038/s41558-020-0694-3

Published on 10 February 2020

Little influence of Arctic amplification on mid-latitude climate

Aiguo Dai[1*] and Mirong Song[2]

Observations[1–3] and model simulations[3,4] show enhanced warming in the Arctic under increasing greenhouse gases, a phenomenon known as the Arctic amplification (AA)[5], that is likely caused by sea-ice loss[1,3]. AA reduces meridional temperature gradients linked to circulation, thus mid-latitude weather and climate changes have been attributed to AA, often on the basis of regression analysis and atmospheric simulations[6–19]. However, other modelling studies[20–22] show only a weak link. This inconsistency may result from deficiencies in separating the effects of AA from those of natural variability or background warming. Here, using coupled model simulations with and without AA, we show that cold-season precipitation, snowfall and circulation changes over northern mid-latitudes come mostly from background warming. AA and sea-ice loss increase precipitation and snowfall above ~60° N and reduce meridional temperature gradients above ~45° N in the lower–mid troposphere. However, minimal impact on the mean climate is seen below ~60° N, with weak reduction in zonal wind over 50°–70° N and 150–700 hPa, mainly over the North Atlantic and northern central Asia. These results suggest that the climatic impacts of AA are probably small outside the high latitudes, thus caution is needed in attributing mid-latitude changes to AA and sea-ice loss on the basis of statistical analyses that cannot distinguish the impact of AA from other correlated changes.

Arctic sea-ice loss and the associated enhanced warming (known as the Arctic amplification or AA) are an integral part of the climate response to increased GHGs. However, due to their large local impacts and potential remote influences, many studies have attempted to quantify the climatic impacts from Arctic sea-ice loss and AA alone. This is often done by running atmospheric general circulation models (AGCMs) forced with low and high sea-ice cover (SIC) and specified sea surface temperatures (SSTs)[10,11,15,20–25], but lately coupled model simulations[26–33] with altered SIC (often by applying an artificial energy flux or through an artificial change in ice albedo[32]) were also used. Besides the amplified warming over the Arctic, the coupled ensemble simulations also show a weak but robust warming over the tropics and an intensification of the winter Aleutian Low and the Siberian High in response to sea-ice loss[32]. However, these responses outside the northern high latitudes are small compared with the total response to GHG forcing[26,27,33].

In contrast to these and other[20–22] modelling studies, which showed weak impacts of Arctic sea-ice loss on Eurasian and North American winter climate, many studies[6–19] have attributed the recent Eurasian winter cooling and cold events to Arctic sea-ice loss and AA, often on the basis of statistical relationships and AGCM simulations. As shown previously[26,27,31], AGCM experiments and statistical relationships can produce misleading results because the SST/SIC forced AGCM experiments are suitable mostly for the tropics due to the importance of the two-way air–sea interactions in the extratropics and the large damping effect from specified SSTs, and a statistical association usually does not imply a cause-and-effect relationship. Further, it is difficult to isolate the real impact of sea-ice loss and the associated AA from that due to the GHG-induced global warming (without AA) by analysing observations or fully coupled model simulations that include both effects[31], especially under large internal variability as seen in individual realizations such as the observations[34]. However, the coupled climate simulations[26–33] contain a strong artificial intervention (for example, by adding a fake energy flux) to the Arctic energy balance whose potential impact is unknown[32]. As a result, the debate continues[16,35].

Here, we explicitly quantify the impact of AA (and the associated sea-ice loss) on mid-latitude mean climate and circulation using novel coupled model simulations (Methods). In our FixedIce simulation, AA is largely suppressed by using a fixed SIC in calculating surface fluxes only, which in turn greatly reduces sea-ice loss compared with the standard 1% CO_2 run (Extended Data Fig. 1). Thus, the FixedIce simulation represents primarily the response due to the background warming without AA, while the difference between the two represents the impact of AA alone. This allows us to quantify and compare the responses to AA and the background warming over the northern mid-latitudes (40°–60° N). Our FixedIce simulation differs from previous coupled simulations[26–33] in its approach to achieve a near-constant SIC and minimum AA (Methods); thus, it provides a cross-validation of the previous model results[32]. Here, we focus on AA's impact on the mean climate during the cold season (October–March), when AA is largest (Extended Data Fig. 1), with its influences on transient weather patterns[35,36] to be investigated later. Results for October–November, December–January and February–March averages are similar, although the zonal wind (U) change becomes significant in December–January at 4×CO_2 around 50°–70° N and 700–200 hPa (Suplementary Fig. 1).

AA and the associated sea-ice loss cause surface air temperature (SAT) and precipitation to increase, mostly over the high latitudes (Fig. 1c), where these SAT and precipitation changes are comparable to those from the GHG forcing alone (Fig. 1b). Northern North America and Northeast Asia also see substantial warming and precipitation increases from AA (Fig. 1c). However, AA does not cause winter cooling over central Asia, as suggested previously, mainly on the basis of regression analysis and AGCM results[6,11]. The AA-induced SAT and precipitation changes over most of 40°–60° N are much smaller than those due to the CO_2 forcing alone (Fig. 1b) and account for only a small fraction (<1/3) of the total response to the CO_2 forcing (Fig. 1a). The warming induced by both the CO_2 forcing and AA causes a reduction in snowfall over most of the mid-latitudes as the freezing line moves northward and

[1]Department of Atmospheric and Environmental Sciences, University at Albany, State University of New York, Albany, NY, USA. [2]LASG, Institute of Atmospheric Physics, Chinese Academy of Sciences, Beijing, China. *e-mail: adai@albany.edu

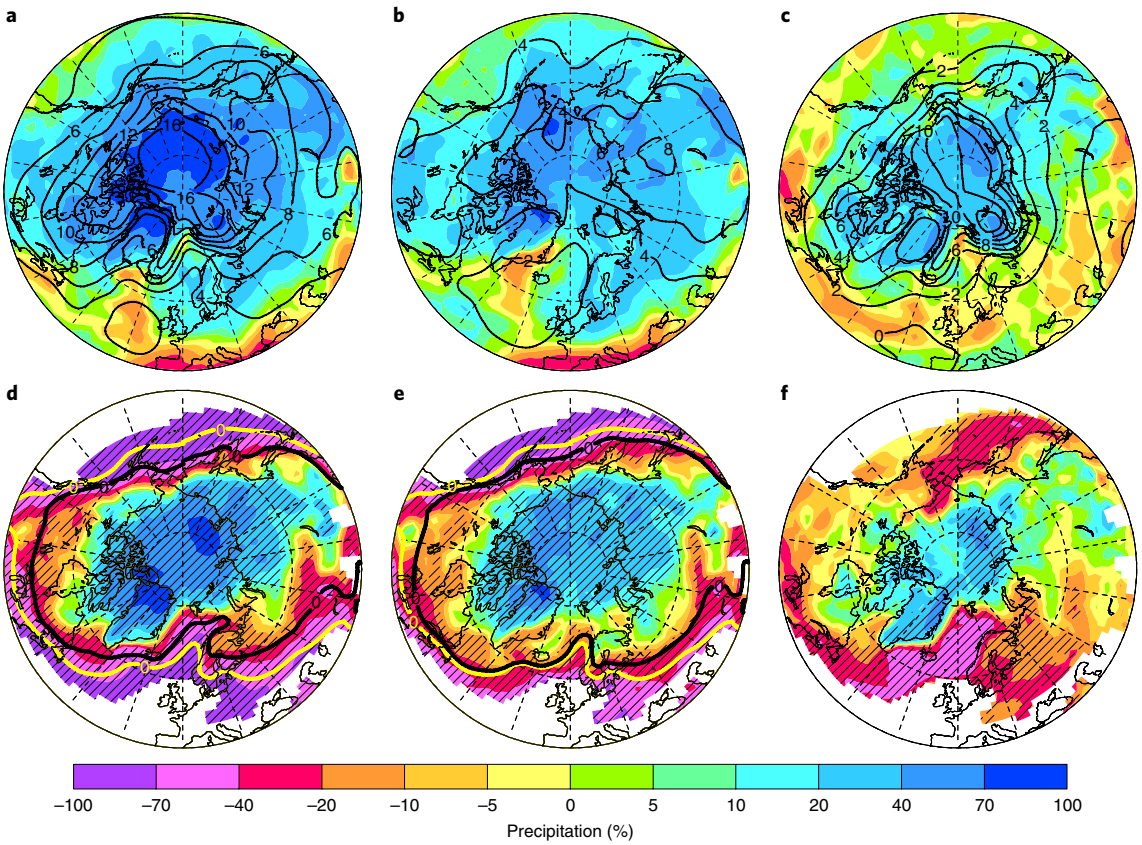

Fig. 1 | Community Earth System Model version 1.2.1 (CESM1) simulated October–March mean changes over 40°–90° N around the time of the second CO_2 doubling. a–c, Precipitation (colour shading, as the percentage of the control climatology) and SAT (contours, in K) changes from the 1% CO_2 (**a**) and FixedIce (**b**) runs and their difference (**a** minus **b**) (**c**). **d–f**, Similar to **a–c** but for the change in snowfall, with the yellow and black lines showing the 0 °C contour line for the control and year 131–150 mean climate, respectively. Areas with less than 0.1 mm day^{-1} snowfall in the control climatology are masked out in **d–f**. All the changes are relative to the control climatology. Hatching in **d–f** indicates the change is statistically significant at the 5% level on the basis of a Student's *t*-test. The temperature changes in **a–c** are all statistically significant, while the precipitation changes over about 20% or below −20% are statistically significant. Panels **a** and **d** represent the total response to the CO_2 forcing; **b** and **e** represent the response to the CO_2 forcing without the Arctic amplification; **c** and **f** represent the impact of the Arctic amplification. This interpretation also applies to other figures. Note the northern mid-latitudes (40°–60° N) are outside the first dashed circle.

more precipitation occurs as rain (Fig. 1d–f). AA does increase snowfall over Greenland substantially and over northern coastal Russia slightly (Fig. 1f); however, the snowfall increase over the northern latitudes (Fig. 1d) comes primarily from the GHG forcing (Fig. 1e) rather than AA (Fig. 1f). Similar results are seen around the first and third CO_2 doubling (Extended Data Figs. 2 and 3). These results contradict some previous studies[6,11,16] that attributed the recent cold and snowy boreal winters mainly to Arctic sea-ice loss on the basis of regression analyses and AGCM results, which could be misleading[27,31].

Increased CO_2 reduces the sea-level pressure (SLP) over the Arctic but increases it over the North Pacific, North Atlantic and Europe (Fig. 2b,e,h) while AA decreases SLP over the North Pacific and northern North America but with small changes over the Arctic (Fig. 2c,f,i). The AA-induced small SLP increases over Eurasia vary with time and are mostly insignificant in our single realization. The total SLP response (Fig. 2a,d,g) is always dominated by the CO_2 forcing over the Arctic and most of the mid-latitudes, with AA's influence becoming evident over northern North America, the North Pacific and Greenland only as CO_2 approaches doubling and quadrupling.

It is often hypothesized that AA could affect mid-latitude circulation by changing atmospheric meridional temperature gradients (dT/dy, where T is tropospheric temperature and y is the meridional distance), which affect U via the thermal wind relation, and U is linked to atmospheric zonal waves and blocking[18,19]. Indeed, AA induces large positive dT/dy changes in the lower–middle troposphere north of ~45° N (Fig. 3c), which reduce the climatological negative dT/dy over this region. Outside this region, AA's influence on dT/dy is small and the CO_2 forcing (Fig. 3b) induces negative (positive) dT/dy changes over the subtropical–midlatitude mid–upper troposphere in the Northern (Southern) Hemisphere, both strengthening the climatological temperature gradients. These CO_2-induced dT/dy changes increase U by 1–7 m s^{-1} (10–20%) over most of the extratropical upper troposphere and throughout the whole troposphere around 50°–80° N and 55°–70° S (Fig. 4b), while AA causes a small and insignificant U decrease in the mid–upper troposphere over 50°–70° N (Fig. 4c). The total U response (Fig. 4a) is dominated by the CO_2-induced change. However, internal variability and time-dependent response may cause the AA's influence estimated from a single realization to differ, as illustrated by the substantial differences in the dT/dy and U changes around the first, second and third CO_2 doublings (Figs. 3 and 4 and Extended Data Figs. 4–7). This makes it difficult to isolate and attribute AA's role in causing mid-latitude circulation changes using observations (which are from one realization). Nevertheless, the U decrease in the mid–upper troposphere over 50°–70° N seen around both the second and third CO_2 doublings (Fig. 4c and Extended Data Fig. 7c)

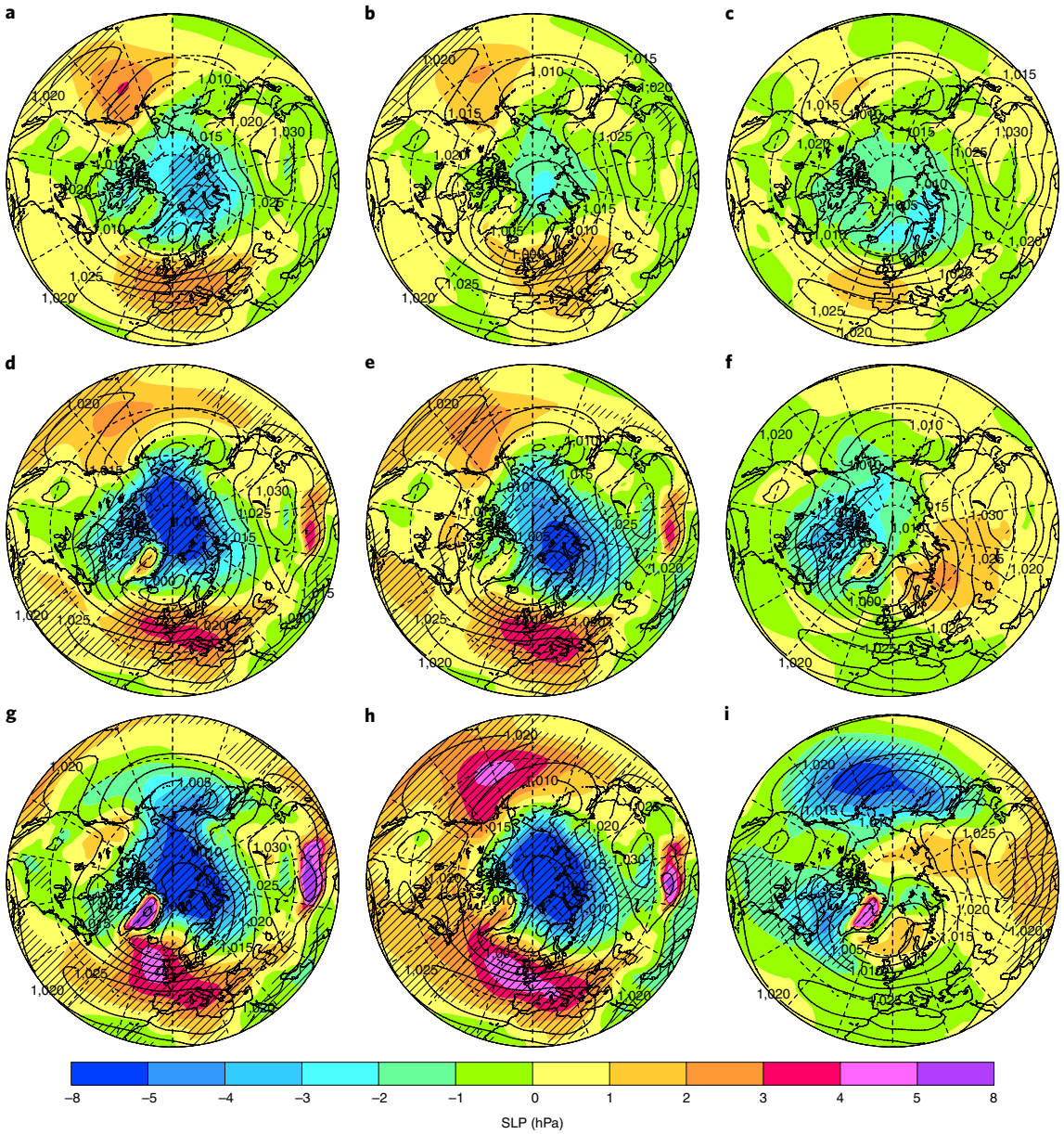

Fig. 2 | CESM1-simualted climatology and changes in October–March mean SLP over 20°–90° N. The SLP climatology (contours) and changes (colour shading, relative to the control run) are in hPa. **a**–**c**, Years 61–80 (first CO_2 doubling); **d**–**f**, years 131–150 (second CO_2 doubling); **g**–**i**, years 201–220 (third CO_2 doubling). **a**,**d**,**g**, The 1% CO_2 run. **b**,**e**,**h**, The FixedIce run. **c**,**f**,**i**, 1% CO_2 minus FixedIce difference. The 20-yr mean SLP (contours) is from the corresponding run in **a**,**b**,**d**,**e**,**g** and **h** and from the control climatology in **c**,**f** and **i**. The hatching indicates the SLP change is statistically significant at the 5% level on the basis of a Student's *t*-test.

appears to be a robust response that is physically consistent with the weakened dT/dy over this region. However, this AA-induced U change would not become significant and detectable before the second CO_2 doubling (CO_2 = 1,139 ppm) and would not be detectable at today's CO_2 level on the basis of these model results. Any forced U changes during the recent periods and the upcoming decades are almost certainly due to the GHG- and aerosol-induced changes, not due to AA. The small dU shown in Fig. 4c over the areas with large dT/dy in the lower–mid troposphere over the mid–high latitudes (Fig. 3c) probably results from the fact that near-surface U is heavily influenced by friction and the thermal wind at a pressure level is proportional to the integral of dT/dy from the surface to that level.

The T and U changes over the northern latitudes (Fig. 5a) exhibit substantial temporal variations that are probably due to internal variability and/or time-dependent response since the external forcing is constant in these simulations, and the dU difference between the 1% CO_2 and FixedIce runs (that is, due to AA) becomes evident only after year 160, despite the large T difference since year 60, as shown by Fig. 5a. The AA-induced U decrease occurs mainly over the North Atlantic and northern central Asia, with small changes (mostly negative) over other parts within 40°–80° N (Fig. 5b).

The main changes in the meridional wind (V) climatological mean are caused by the CO_2 forcing rather than AA. They include an upward shift of the maximum V in the upper tropical troposphere and a small but significant increase of ~0.2 m s^{-2} at 2 × CO_2 and ~0.4 m s^{-2} at 4 × CO_2 in the lower troposphere over 50°–80° N (Extended Data Figs. 8b and 9b), while the AA-induced V changes are small, with small decreases of 0.1–0.2 m s^{-1} over 50°–85° N only

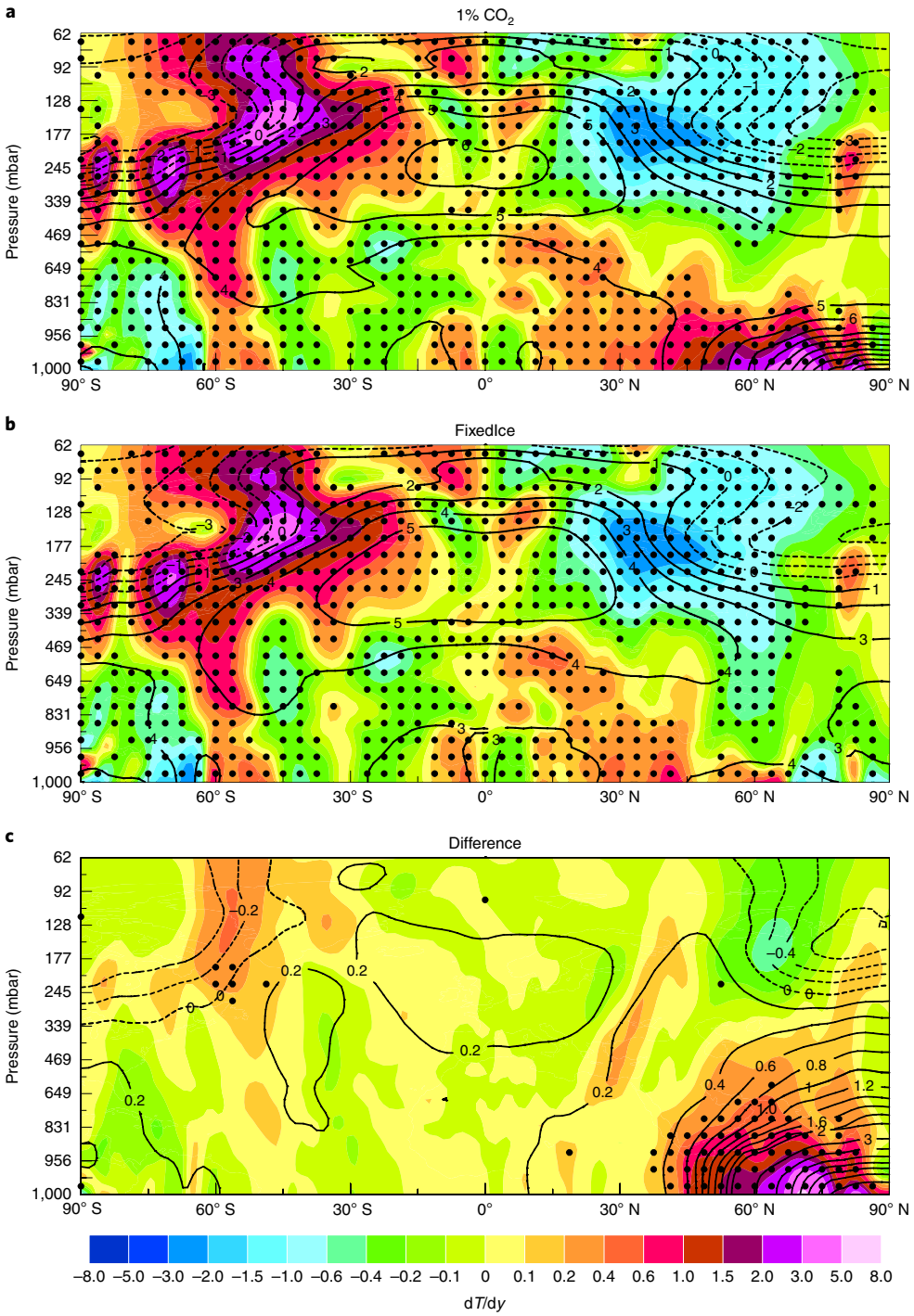

Fig. 3 | CESM1-simualted changes around the time of the second CO_2 doubling in October–March zonal-mean air temperature and its meridional gradient. a,**b**, Changes (relative to the control run) in air temperature (contours, in K) and temperature gradient (d*T*/d*y*, colour shading, in K per 10° latitude) from the 1% CO_2 run (**a**) and the FixedIce run (**b**). **c**, The **a** minus **b** difference. Most of the temperature changes in **a** and **b** are statistically significant at the 5% level, while the significant changes in the temperature gradient are marked by the black dots. The temperature differences shown in **c** are mostly insignificant outside the lower–mid troposphere north of about 45° N (similar to the *P* value of the d*T*/d*y* difference). Results are similar for October–November, December–January and February–March averages.

by the time of 8×CO_2 (Extended Data Fig. 9c). AA-induced *V* changes at many locations vary with time and do not always have the same sign as the current climatology (Supplementary Figs. 4 and 5). Thus, the *V* changes do not always enhance current *V*. These results suggest that any forced *V* changes, including possible strengthening over 50°–80° N, in the recent and upcoming decades are probably caused by the GHG forcing rather than AA. In fact, the AA may weaken the *V* over the northern latitudes (Extended Data Fig. 9c), which is the opposite to the hypothesized strengthening of the meridional circulation due to AA[17].

Our AA-induced SAT, SLP and *U* changes are broadly consistent with those reported previously;[26–33] however, because of the

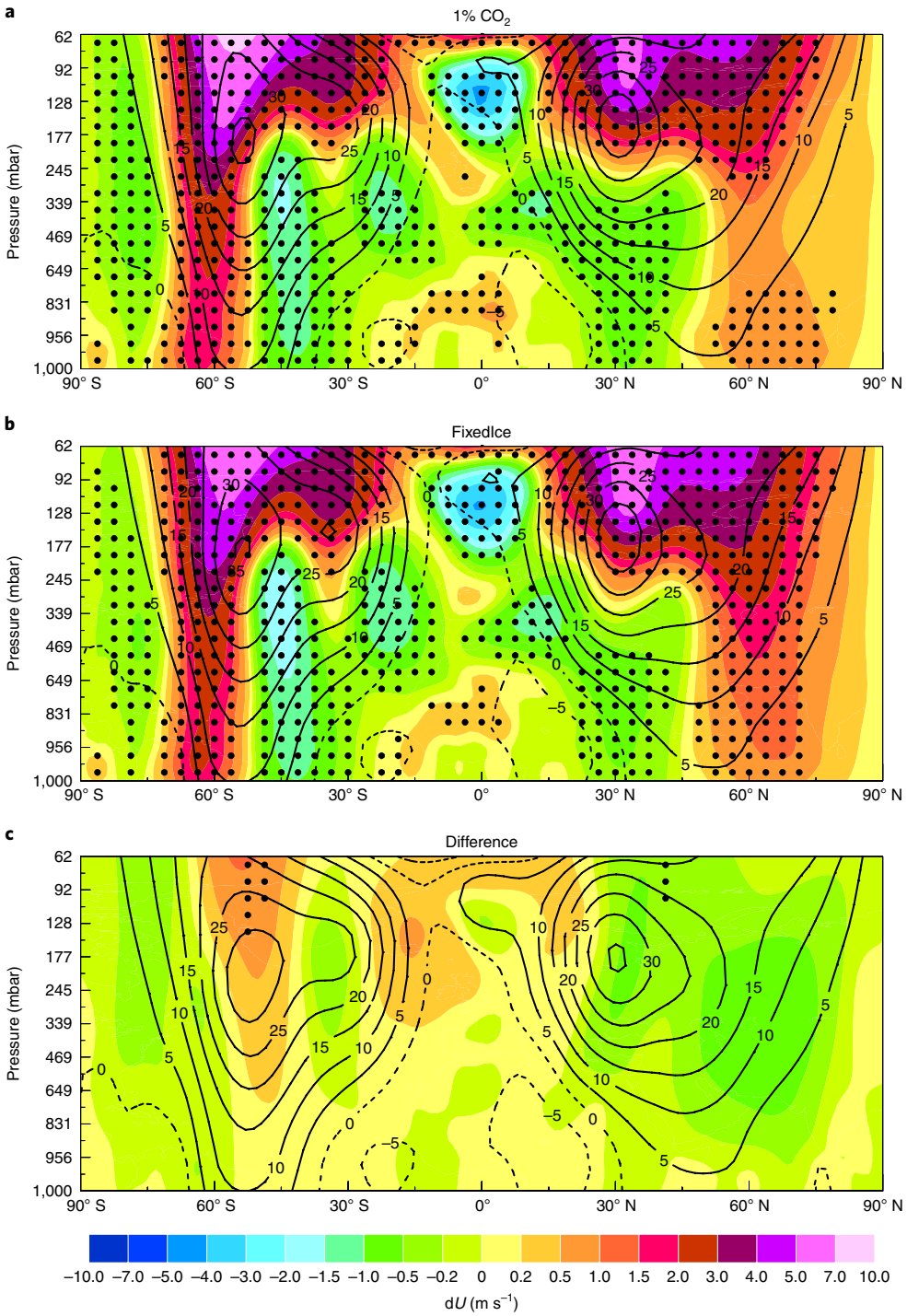

Fig. 4 | CESM1-simualted climatology and changes averaged over years 131–150 in October–March zonal-mean *U*. **a**,**b**, Climatology (contours, in m s^{-1}, for years 131–150) and changes (colour, in m s^{-1}, relative to control run) from the 1% CO_2 run (**a**) and FixedIce run (**b**). **c**, The **a** minus **b** difference. Significant wind changes in **a** and **b** and differences in **c** at the 5% level are marked by the black dots. The contours in **c** are for the control-run climatology of *U*. Results are similar for October–November, December–January and February–March averages.

improved design of the experiments, we were able to explicitly show that these changes are small compared with the total response to CO_2 forcing, and they are mostly insignificant outside the high latitudes in individual realizations. Our modelling results suggest that any forced changes outside the northern high latitudes in the recent and upcoming decades are more likely due to GHG-induced climate change rather than a response to AA and the concurring sea-ice loss. They also suggest that statistical correlations with and regression-explained variance by sea-ice loss for both inter-annual variations and long-term trends may not imply that sea-ice loss is a cause. In fact, they are both probably caused by the same GHG forcing or other short-term processes. The response to the amplified Arctic warming alone cannot be easily quantified from observations or model simulations that include both effects from GHG-induced global warming and AA, and responses simulated by AGCMs may be unrealistic. Thus, caution must be exercised in attributing

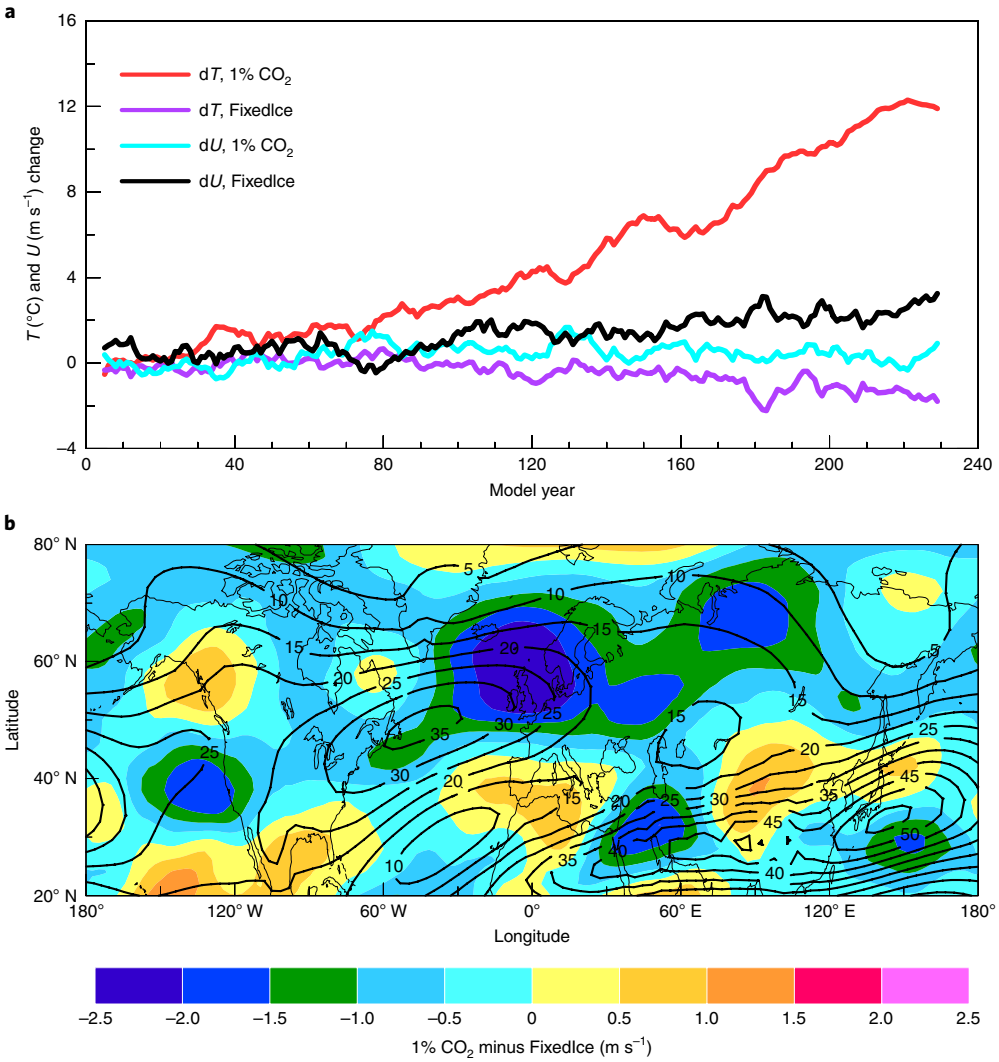

Fig. 5 | Differences in lower-tropospheric temperature and tropospheric *U* between high and mid-latitudes and spatial patterns of *U* changes around 266 hPa. a, Eleven-year smoothed October–March mean changes (relative to the mean of years 1–30 from the 1% CO_2 run) in the lower tropospheric (~831–1,000 hPa) zonal-mean temperature difference between 70°–90° N and 30°–50° N from the 1% CO_2 run (red) and FixedIce run (magenta), and in tropospheric (~208–831 hPa) mean *U* averaged over 50°–70° N from the 1% CO_2 run (blue) and FixedIce run (black). **b**, Spatial distribution of the 1% CO_2 minus FixedIce difference (colour, in m s^{-1}) in October–March mean *U* at a level around 266 hPa averaged over years 131–150. The contours are the mean *U* (in m s^{-1}) from the control run.

recent weather and climate changes over northern mid-latitudes to Arctic sea-ice loss and AA on the basis of statistical analyses of data. This is because such data include both effects from AA and the GHG-induced background warming, and these effects and that from internal variability cannot be easily separated in such analyses.

Here we examined only AA's impact on the mean climate response to CO_2 increases during the cold season from October to March. Further analyses are needed to quantify AA's impacts on transient weather patterns such as the Ural blocking[18,19] or climate variability over the northern mid-latitudes as many previous studies suggest that most Arctic–mid-latitude linkages are regional and episodic, with timescales of weeks to a few months[35,36]. Nevertheless, the results presented here suggest that these regional and episodic linkages are unable to produce significant impacts on the seasonal mean fields, such as the winter cooling over Eurasia seen in recent decades[2]. It is possible that the CESM1 model may have failed to simulate AA's impact on transient weather. However, many previous studies were unable to separate AA's impact from that resulting from natural variability or the background global warming and thus may have incorrectly attributed recent changes in transient weather patterns to AA. We are currently analysing daily data from the CESM1 simulations to address these issues.

Historical Arctic warming rates are correlated with the Atlantic Multi-decadal Oscillation (AMO)[37], and the recent accelerated warming and sea-ice loss in the Barents-Kara Seas (BKS)[1] are linked to increased intrusion of North Atlantic warm water[38] associated with a warm AMO phase. Since the recent AMO cycles result from either natural variability or historical aerosol forcing[39], a large part of the recent BKS warming and sea-ice loss and the associated impact on atmospheric circulation[18,19] and the cooling effect over Eurasia[40] may be unrelated to GHG-induced Arctic warming and sea-ice loss. This could help reconcile the modelling results of little influence from GHG-induced AA and sea-ice loss on the mid-latitudes and the previous analyses[6–19] linking recent Eurasian cooling to BKS warming and sea-ice loss, as the latter may be mainly looking at AMO-induced BKS warming and sea-ice loss together with AMO-induced atmospheric circulation changes that likely differ from GHG-induced changes.

Online content

Any methods, additional references, Nature Research reporting summaries, source data, extended data, supplementary information, acknowledgements, peer review information; details of author contributions and competing interests; and statements of data and code availability are available at https://doi.org/10.1038/s41558-020-0694-3.

Received: 23 January 2019; Accepted: 8 January 2020;
Published online: 10 February 2020

References

1. Screen, J. A. & Simmonds, I. The central role of diminishing sea-ice in recent Arctic temperature amplification. *Nature* **464**, 1334–1337 (2010).
2. Cohen, J. et al. Recent Arctic amplification and extreme mid-latitude weather. *Nat. Geosci.* **7**, 627–637 (2014).
3. Dai, A., Luo, D., Song, M. & Liu, J. Arctic amplification is caused by sea-ice loss under increasing CO_2. *Nat. Commun.* **10**, 121 (2019).
4. Barnes, E. A. & Polvani, L. M. CMIP5 projections of Arctic amplification, of the North American/North Atlantic circulation, and of their relationship. *J. Clim.* **28**, 5254–5271 (2015).
5. Serreze, M. C. & Barry, R. G. Processes and impacts of Arctic amplification: a research synthesis. *Glob. Planet. Change* **77**, 85–96 (2011).
6. Liu, J., Curry, J. A., Wang, H., Song, M. & Horton, R. M. Impact of declining Arctic sea ice on winter snowfall. *Proc. Natl Acad. Sci. USA* **109**, 4074–4079 (2012).
7. Overland, J., Wood, K. R. & Wang, M. Warm Arctic—cold continents: climate impacts of the newly open Arctic Sea. *Polar Res.* **30**, 15787 (2011).
8. Screen, J. A. & Simmonds, I. Exploring links between Arctic amplification and mid-latitude weather. *Geophys. Res. Lett.* **40**, 959–964 (2013).
9. Walsh, J. E. Intensified warming of the Arctic: causes and impacts on middle latitudes. *Glob. Planet. Change* **117**, 52–63 (2014).
10. Mori, M., Watanabe, M., Shiogama, H., Inoue, J. & Kimoto, M. Robust Arctic sea-ice influence on the frequent Eurasian cold winters in past decades. *Nat. Geosci.* **7**, 869–873 (2014).
11. Mori, M., Kosaka, Y., Watanabe, M., Nakamura, H. & Kimoto, M. A reconciled estimate of the influence of Arctic sea-ice loss on recent Eurasian cooling. *Nat. Clim. Change* **9**, 123–129 (2019).
12. Francis, J. A. & Vavrus, S. J. Evidence for a wavier jet stream in response to rapid Arctic warming. *Environ. Res. Lett.* **10**, 014005 (2015).
13. Kug, S.-W. et al. Two distinct influences of Arctic warming on cold winters over North America and East Asia. *Nat. Geosci.* **8**, 759–762 (2015).
14. Kretschmer, M. D., Coumou, J. F. D. & Runge, J. Using causal effect networks to analyze different Arctic drivers of midlatitude winter circulation. *J. Clim.* **29**, 4069–4081 (2016).
15. Meleshko, V. et al. Arctic amplification: does it impact the polar jet stream? *Tellus A* **68**, 32330 (2016).
16. Francis, J. A. Why are Arctic linkages to extreme weather still up in the air? *Bull. Am. Meteorol. Soc.* **98**, 2551–2557 (2017).
17. Francis, J. A., Vavrus, S. J. & Cohen, J. Amplified Arctic warming and mid-latitude weather: new perspectives on emerging connections. *WIREs Clim. Change* **8**, e474 (2017).
18. Yao, Y., Luo, D., Dai, A. & Simmonds, I. Increased quasi-stationarity and persistence of Ural blocking and Eurasian extreme cold events in response to Arctic warming. Part I: insights from observational analyses. *J. Clim.* **30**, 3549–3568 (2017).
19. Luo, D., Chen, X., Dai, A. & Simmonds, I. Changes in atmospheric blocking circulations linked with winter Arctic sea-ice loss: a new perspective. *J. Clim.* **31**, 7661–7678 (2018).
20. Chen, H. W., Zhang, F. & Alley, R. B. The robustness of midlatitude weather pattern changes due to Arctic sea ice loss. *J. Clim.* **29**, 7831–7849 (2016).
21. McCusker, K. E., Fyfe, J. C. & Sigmond, M. Twenty-fve winters of unexpected Eurasian cooling unlikely due to arctic sea ice loss. *Nat. Geosci.* **9**, 838–842 (2016).
22. Sun, L., Perlwitz, J. & Hoerling, M. What caused the recent "warm Arctic, cold continents" trend pattern in winter temperatures? *Geophys. Res. Lett.* **43**, 5345–5352 (2016).
23. Deser, C., Tomas, R. A., Alexander, M. & Lawrence, D. The seasonal atmospheric response to projected Arctic sea ice loss in the late twenty-first century. *J. Clim.* **23**, 333–351 (2010).
24. Sun, L., Deser, C. & Tomas, R. A. Mechanisms of stratospheric and tropospheric circulation response to projected Arctic sea ice loss. *J. Clim.* **28**, 7824–7845 (2015).
25. Screen, J. A. Simulated atmospheric response to regional and pan-Arctic sea ice loss. *J. Clim.* **30**, 3945–3962 (2017).
26. Deser, C., Tomas, R. A. & Sun, L. The role of ocean–atmosphere coupling in the zonal-mean atmospheric response to Arctic sea ice loss. *J. Clim.* **28**, 2168–2186 (2015).
27. Deser, C., Sun, L., Tomas, R. A. & Screen, J. Does ocean coupling matter for the northern extratropical response to projected Arctic sea ice loss? *Geophys. Res. Lett.* **43**, 2149–2157 (2016).
28. Blackport, R. & Kushner, P. J. Isolating the atmospheric circulation response to Arctic sea ice loss in the coupled climate system. *J. Clim.* **30**, 2163–2185 (2017).
29. McCusker, K. E. et al. Remarkable separability of circulation response to Arctic sea ice loss and greenhouse gas forcing. *Geophys. Res. Lett.* **44**, 7955–7964 (2017).
30. Oudar, T. et al. Respective roles of direct GHG radiative forcing and induced Arctic sea ice loss on the Northern Hemisphere atmospheric circulation. *Clim. Dynam.* **49**, 3693–3713 (2017).
31. Smith, D. M. et al. Atmospheric response to Arctic and Antarctic sea ice: the importance of ocean–atmosphere coupling and the background state. *J. Clim.* **30**, 4547–4565 (2017).
32. Screen, J. A. et al. Consistency and discrepancy in the atmospheric response to Arctic sea-ice loss across climate models. *Nat. Geosci.* **11**, 155–163 (2018).
33. Sun, L., Alexander, M. & Deser, C. Evolution of the global coupled climate response to Arctic sea ice loss during 1990–2090 and tts contribution to climate change. *J. Clim.* **31**, 7823–7843 (2018).
34. Dai, A. & Bloecker, C. E. Impacts of internal variability on temperature and precipitation trends in large ensemble simulations by two climate models. *Clim. Dynam.* **52**, 289–306 (2019).
35. Cohen, J. et al. Divergent consensuses on Arctic amplification influence on midlatitude severe winter weather. *Nat. Clim. Change* **10**, 20–29 (2020).
36. Overland, J. E. et al. Nonlinear response of mid-latitude weather to the changing Arctic. *Nat. Clim. Change* **6**, 992–999 (2016).
37. Chylek, P., Folland, C. K., Lesins, G., Dubey, M. K. & Wang, M. Arctic air temperature change amplification and the Atlantic Multidecadal Oscillation. *Geophys. Res. Lett.* **36**, L14801 (2009).
38. Spielhagen, R. F. et al. Enhanced modern heat transfer to the Arctic by warm Atlantic water. *Science* **331**, 450–453 (2011).
39. Hua, W., Dai, A., Zhou, L., Qin, M. & Chen, H. An externally-forced decadal rainfall seesaw pattern over the Sahel and southeast Amazon. *Geophys. Res. Lett.* **46**, 923–932 (2019).
40. Luo, D. et al. Winter Eurasian cooling linked with the Atlantic Multidecadal Oscillation. *Environ. Res. Lett.* **12**, 125002 (2017).

Methods

CESM1 simulations. The model simulations used here were taken from Dai et al.[3], who described and evaluated them in detail. Here we briefly describe them, using some text from ref. [3]. We used the CESM1[41] from the National Center for Atmospheric Research with version 4 of the Community Atmosphere Model (CAM4) for its atmospheric component. The CESM1 was run with grid spacing of 2.5° longitude × ~2.0° latitude for the atmospheric model, and ~1.0° longitude × ~0.5° latitude for the sea-ice and ocean models. Previous studies[3,26,42] have shown that the CESM1 simulates the Arctic mean climate fairly realistically, including the spatial and seasonal patterns of the sea ice and surface fluxes. We compared the standard deviations (s.d.) of the monthly fields examined here in CESM1 historical simulations with those from the European Centre for Medium-range Weather Forecasts (ECMWF) re-analysis (ERA-) Interim reanalysis during 1979–2016 and found that the CESM1 has generally realistic variability for the monthly fields examined here, although noticeable differences exist in the s.d. patterns for sea-level pressure and precipitation (Supplementary Figs. 2 and 3).

We made two multi-century simulations plus a 150-year pre-industrial control run (CTL, with CO_2 fixed at 284.7 ppmv). The first multi-century simulation is a standard 1% yr^{-1} CO_2 increase run (1% CO_2) with fully coupled dynamic sea ice for 235 years, until atmospheric CO_2 reaches 10.36 times the pre-industrial CO_2 level. The second run (referred to as FixedIce) is the same as the 1% CO_2 run except that all the internally calculated ice–atmosphere, ice–ocean and ocean–atmosphere fluxes north of 30° N were applied to the fixed sea-ice fractional areas temporally interpolated from the monthly climatology of the CTL run. This differs from the standard 1% CO_2 run in which these fluxes were applied only to the ice faction that existed at the time in the model (Extended Data Fig. 10). Over a small fraction of the Arctic sea-ice area north of 30° N (mainly along the sea-ice margins at lower latitudes, see supplementary figure S9 in ref. [3]), sea ice melted away completely (mainly in the latter part of the simulation), and thus the ice model did not calculate these fluxes. For these small areas, we used the monthly climatology of these fluxes from the CTL run (after the temporal interpolation to the day within the month), except for surface-absorbed shortwave (SW) radiation, which was calculated using the CTL albedo values and model-internally calculated downward SW radiation. The CTL ice–atmosphere fluxes (including latent and sensible heat fluxes, evaporation, upward longwave radiation and surface stress) and ice–ocean fluxes (including heat, salt, freshwater, SW radiation and stress fluxes) did not account for long-term changes in surface temperatures and other fields; thus, they could potentially suppress long-term changes in the Arctic if applied widely. However, the CTL fluxes were used only over a very small fraction of the total sea-ice area along the initial ice margins where SIC was low at the start and melted away completely (see supplementary fig. S9 in ref. [3]); thus, the effect of this deficiency is likely to be small.

In the FixedIce run, the coupler and the atmospheric and ocean components in the CESM1 saw only the fixed sea-ice cover interpolated from the CTL run north of 30° N; the sea-ice fraction inside the sea-ice model was allowed to evolve dynamically with the fluxes returned from the coupler. Thus, the preceding changes made in the FixedIce run would also affect the rate of sea-ice loss through the modification to the surface fluxes (Extended Data Fig. 10).

The difference between the standard 1% CO_2 and FixedIce runs comes mainly from the application of the internally calculated fluxes over a sea-ice surface to different sea-ice fractions: in the 1% CO_2 run, the fluxes were applied to the actual ice cover or the fraction existed in the model at the time; in the FixedIce run, they were applied to a fixed ice cover (with a fixed seasonal cycle) derived from the CTL run (Extended Data Fig. 10). This is equivalent to changing the ocean surface type (our main intervention) for the purpose of air–sea flux calculations from open water in the 1% CO_2 run to sea-ice cover in the FixedIce run for many of the Arctic grid boxes. Clearly, this artificial surface-type change can lead to large changes in the calculated surface fluxes, but the basic energy and mass conservations are still preserved in the flux calculations. However, by applying the ice–atmosphere and ice–ocean energy and water fluxes from the actual ice fraction to the CTL fraction (Extended Data Fig. 10), we may have extended the small energy sink, and freshwater release occurred within the actual ice fraction to a larger area; this expanded energy sink and freshwater source are artificial and not accounted for in the FixedIce run. As shown by Extended Data Fig. 1 and supplementary fig. S9 in ref. [3], however, the SIC difference between the internally calculated and CTL-derived values is small in the FixedIce run for the years before the time of CO_2 quadrupling. Thus, the effect of this deficiency is also likely to be small, at least for the early part (<150 years) of the simulation. The initial SIC of the FixedIce run was taken from the same control run; thus, it remained similar to the CTL-derived values during the early part of the simulation because sea-ice melting was small as the altered surface fluxes suppressed AA and Arctic warming in the FixedIce run.

Our approach here focuses on the effects on the climate (including sea ice itself) of a fixed sea-ice cover through its impact on surface fluxes, and by doing so it also largely eliminates the Arctic amplification of warming (Extended Data Fig. 1). It differs from previous studies[26–33] in the way to maintain a near-constant SIC. For example, Deser et al.[26,27] used an artificial longwave forcing, McCusker et al.[29] and Sun et al.[33] added a 'ghost energy flux' to the ice model, Blackport and Kushner[29] modified ice albedo, Oudar et al.[30] applied a heat flux to the ocean model and Smith et al.[31] essentially reset the SIC to a target value (which could lead to unlimited sea-ice melting and release of freshwater). By comparison, our approach, which is essentially a change of ocean surface type, has relatively low artificial intervention of the Arctic climate system. As Arctic warming under rising CO_2 is sensitive to how the coupled atmosphere–ocean–ice processes are simulated[43], one could argue that it is better to achieve a near-constant sea-ice cover with as little artificial intervention as possible. We also focus on the transient response to a graduated CO_2 increase in an individual realization, which resembles the real world. By contrast, most of the previous studies focused on the ensemble mean response, which contains reduced internal variability and thus is a more robust estimate of the response but is not comparable to observations.

Student's *t*-tests and a 5% significance level were applied to test whether a change in the mean of a given climate variable is statistically significant throughout the study.

Data availability

The model data used in this study are available from the authors upon request.

References

41. Hurrell, J. W. et al. The Community Earth System Model: a framework for collaborative research. *Bull. Am. Meteorol. Soc.* **94**, 1339–1360 (2013).
42. Jahn, A. et al. Late-twentieth-century simulation of Arctic sea ice and ocean properties in the CCSM4. *J. Clim.* **25**, 1431–1452 (2012).
43. Boeke, R. C. & Taylor, P. C. Seasonal energy exchange in sea ice retreat regions contributes to differences in projected Arctic warming. *Nat. Commun.* **9**, 5017 (2018).

Acknowledgements

We thank J. Liu for constructive discussions regarding the design and impact of the FixedIce run. M.S. was supported by the Chinese Academy of Sciences Strategic Priority Research Program (grant no. XDA19070403). A.D. was supported by the National Science Foundation (grant nos. AGS-1353740 and OISE-1743738), the US Department of Energy's Office of Science (grant no. DE-SC0012602) and the US National Oceanic and Atmospheric Administration (grant nos. NA15OAR4310086 and NA18OAR4310425).

Author contributions

A.D. designed the research and performed the numerical experiments and analyses. M.S. helped make the necessary code changes for the FixedIce run.

Competing interests

The authors declare no competing interests.

Additional information

Extended data is available for this paper at https://doi.org/10.1038/s41558-020-0694-3.

Supplementary information is available for this paper at https://doi.org/10.1038/s41558-020-0694-3.

Correspondence and requests for materials should be addressed to A.D.

Peer review information *Nature Climate Change* thanks Patrick Taylor, Robert Tomas and the other, anonymous, reviewer(s) for their contribution to the peer review of this work.

Reprints and permissions information is available at www.nature.com/reprints.

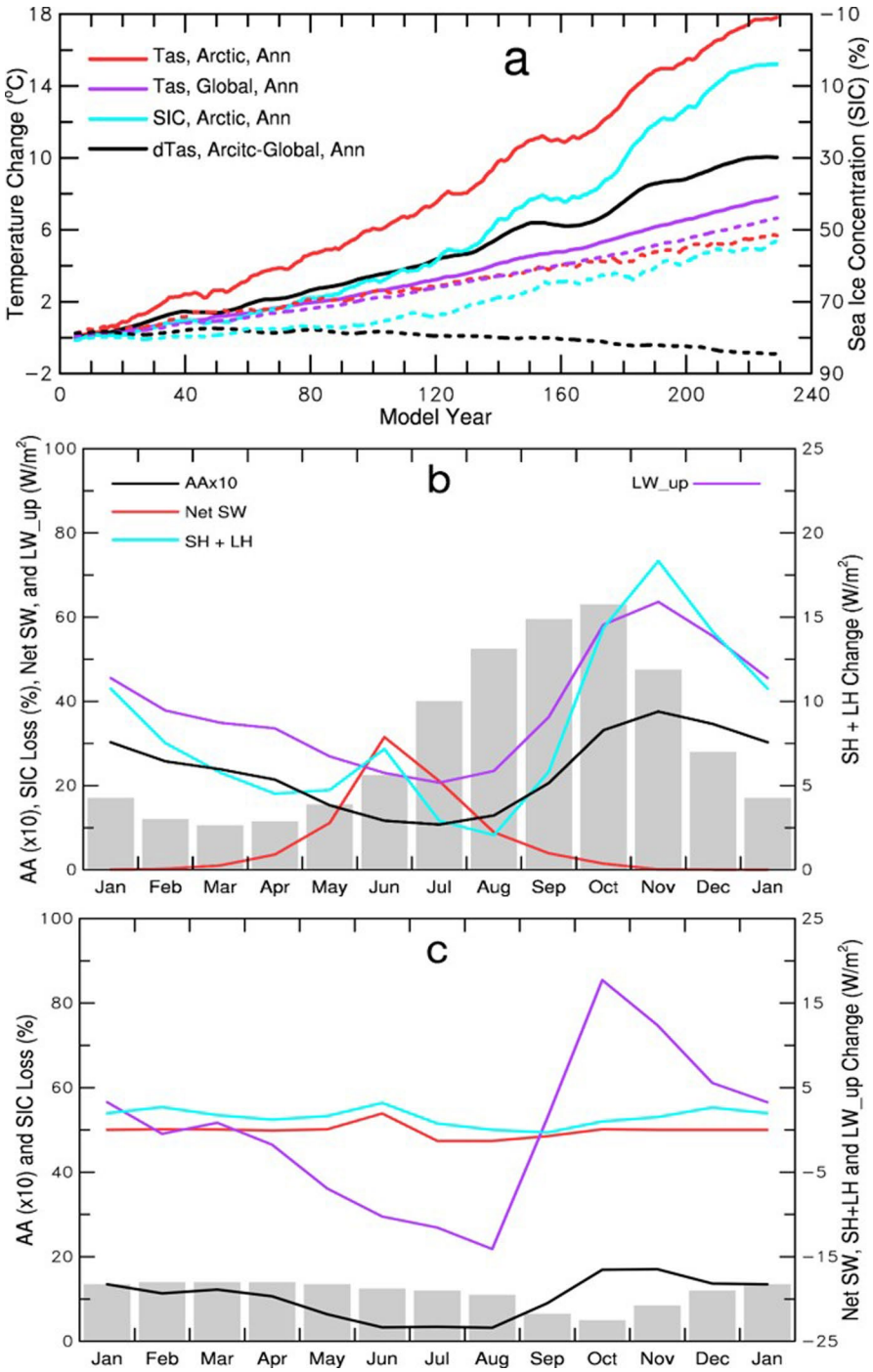

Extended Data Fig. 1 | CESM1-somulated Arctic sea-ice, temperature and flux changes. (**a**) Eleven-year-moving averaged time series of the changes (relative to the control-run climatology) in Arctic (67°–90°N, red) and global-mean (magenta) annual surface air temperature (Tas), Arctic-minus-global annual Tas difference (black), and Arctic annual sea-ice concentration (SIC, blue) from the 1% CO2 run (solid lines) and FixedIce run (dashed lines). (**b**, **c**) CESM1-simulated changes (relative to the control-run climatology) averaged over years 131–150 as a function of month in Arctic sea-ice concentration (SIC, in % area, gray bars) and surface net shortwave (SW) radiation (red), upward longwave (LW) radiation (magenta), and sensible plus latent heat fluxes (blue) from the (**b**) 1% CO2 run and (**c**) FixedIce run.

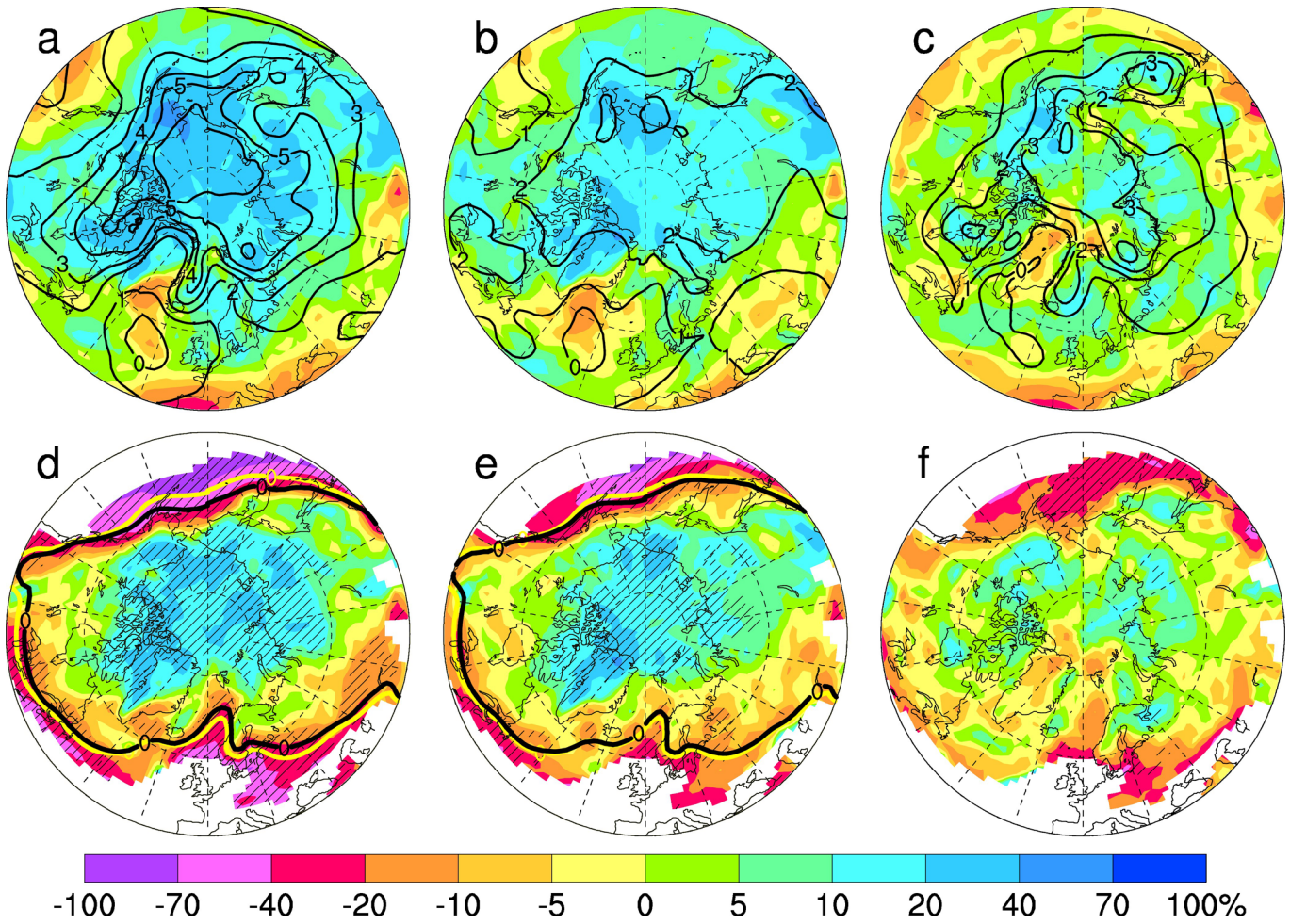

Extended Data Fig. 2 | CESM1-simualted October-March mean changes over 40°–90°N around the time of the 1st CO2 doubling (that is, for years 61–80). Same as Fig. 1 but at the time of the 1st CO2 doubling (that is, for year 61–80 mean).

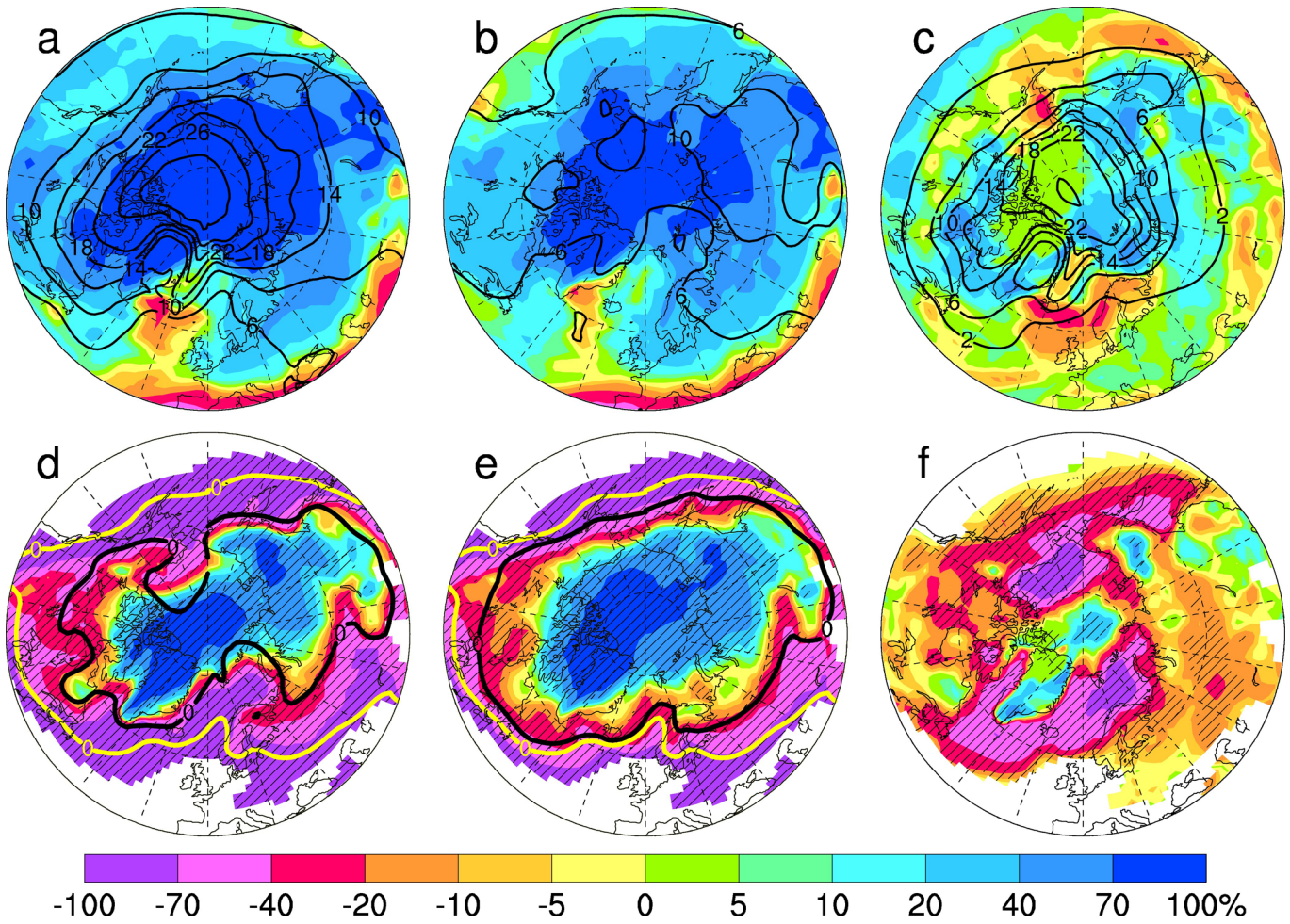

Extended Data Fig. 3 | CESM1-simualted October-March mean changes over 40°–90°N around the time of the 3rd CO2 doubling (that is, for years 201–220). Same as Fig. 1 but around the 3rd CO2 doubling (that is, for year 201–220 mean).

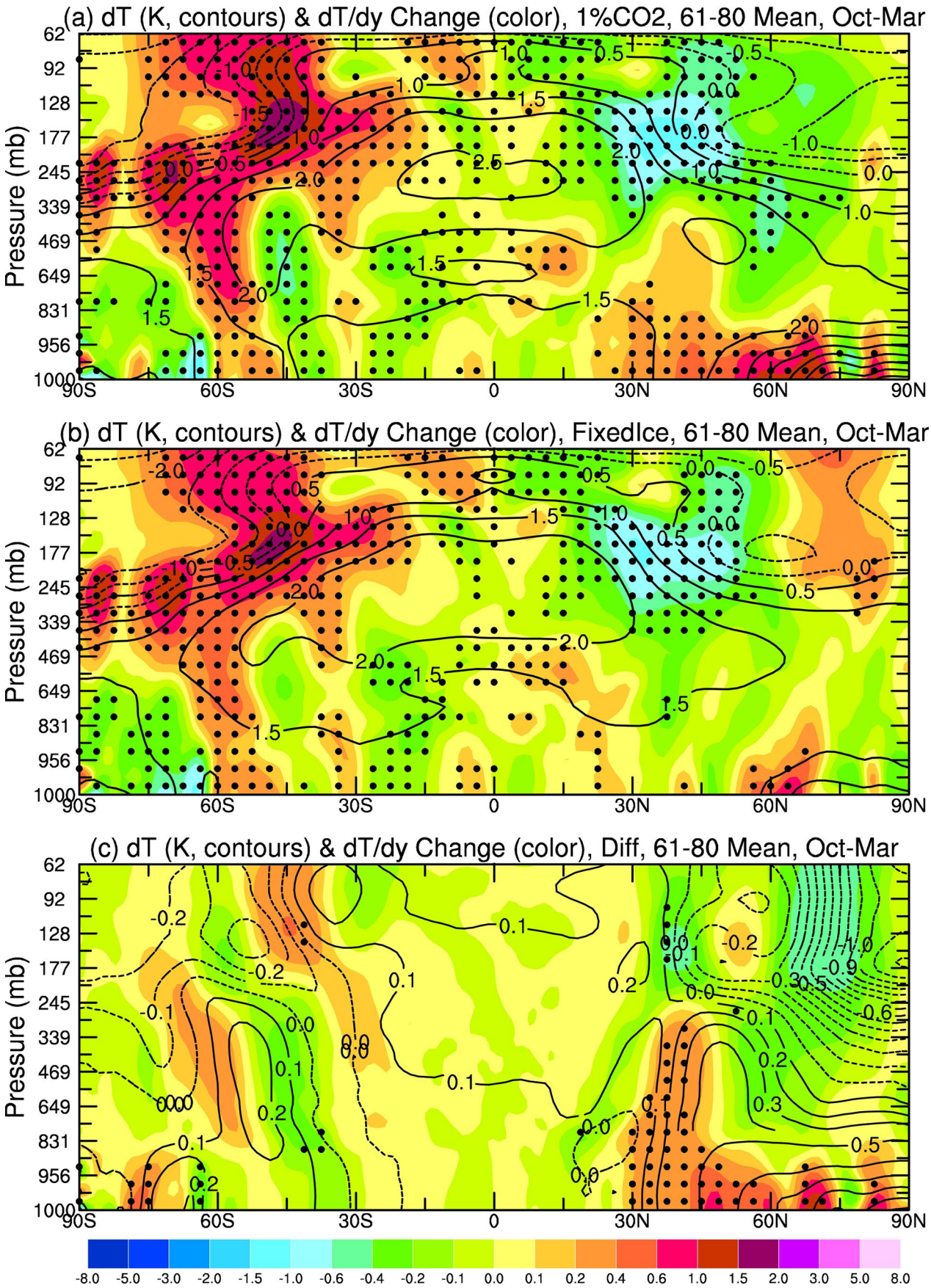

Extended Data Fig. 4 | CESM1-simualted changes in zonal-mean temperature around the time of the 1st CO2 doubling (that is, for years 61–80). Same as Fig. 3 but around the time of the 1st CO2 doubling (that is, for years 61–80).

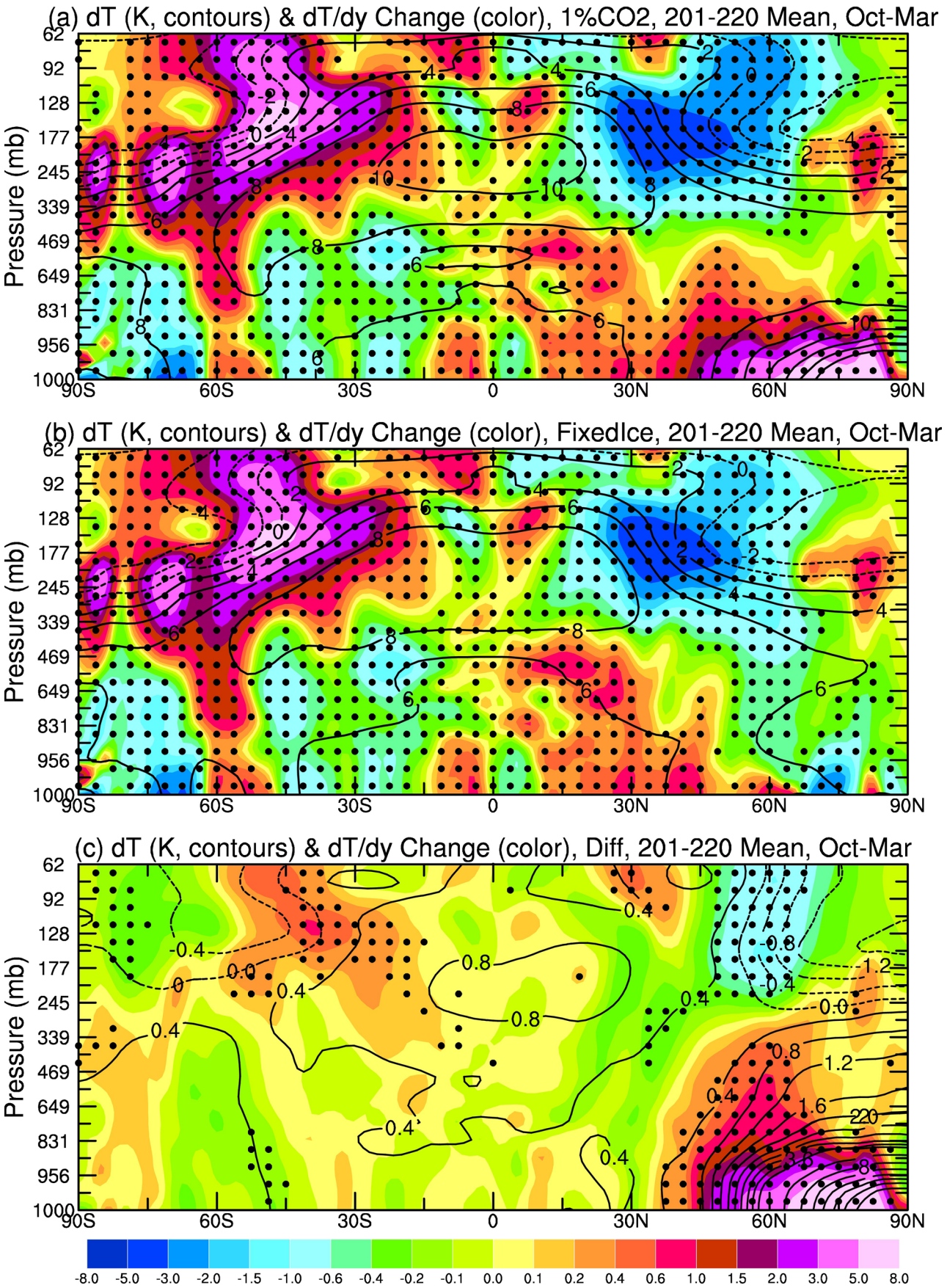

Extended Data Fig. 5 | CESM1-simualted changes in zonal-mean temperature around the time of the 3rd CO2 doubling (that is, for years 201–220). Same as Fig. 3 but around the time of the 3rd CO2 doubling (that is, for years 201–220).

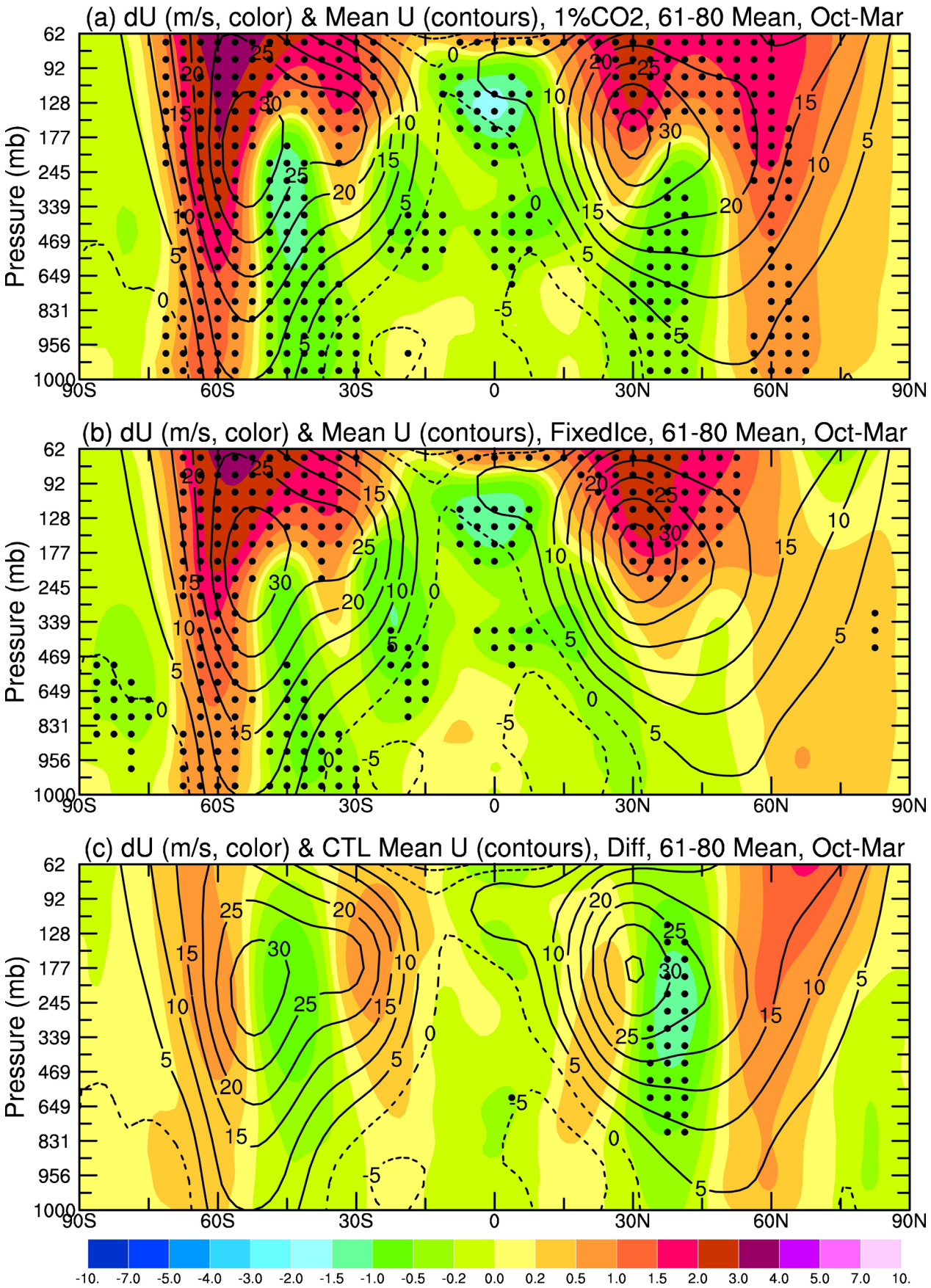

Extended Data Fig. 6 | CESM1-simulated climatology (contours) and changes (color) in October-March zonal-mean U wind around the 1st CO2 doubling (that is, for years 61–80). Same as Fig. 4 but around the time of the 1st CO2 doubling (that is, for years 61–80).

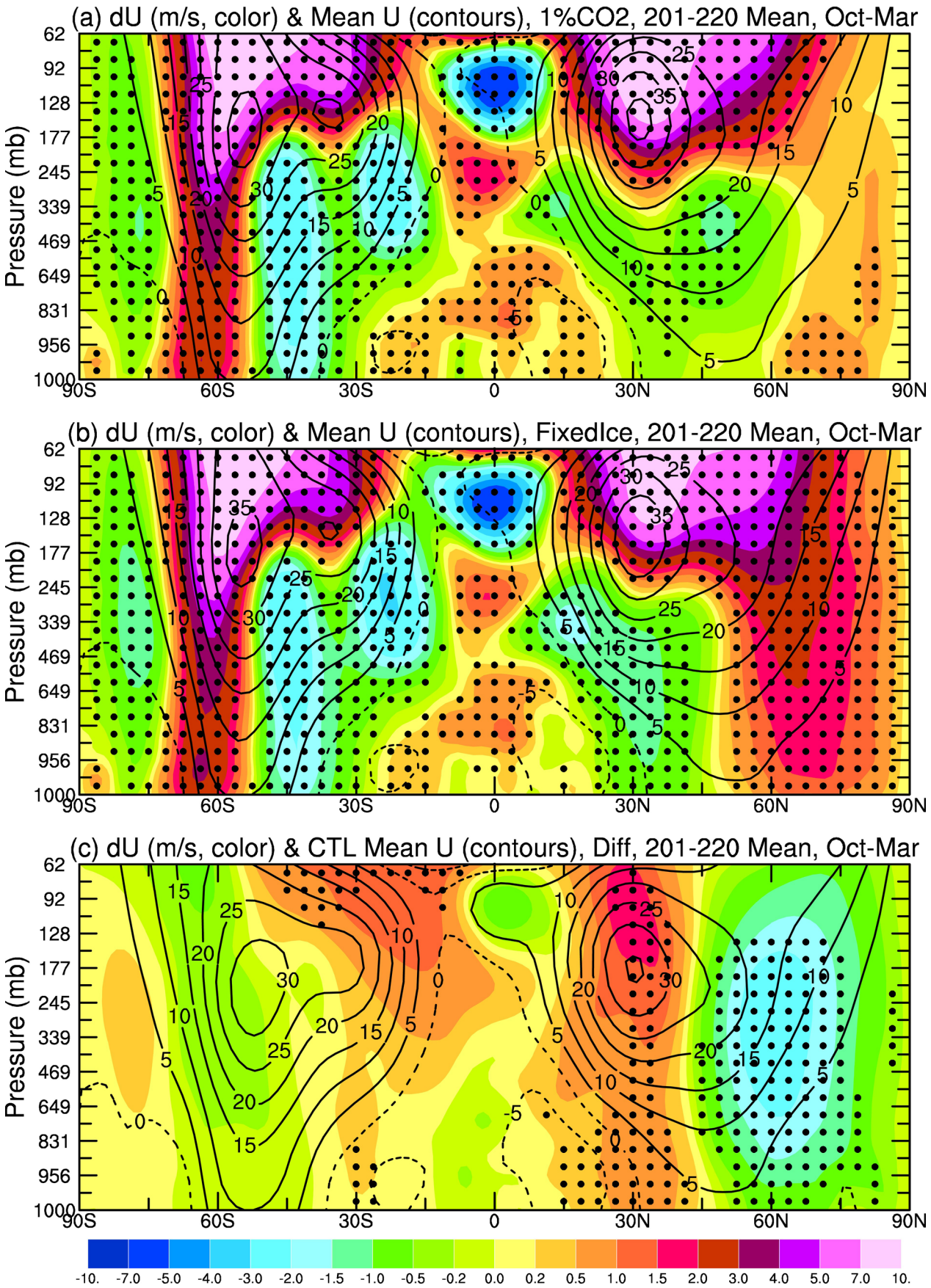

Extended Data Fig. 7 | CESM1-simulated climatology (contours) and changes (color) in October-March zonal-mean U wind around the 3rd CO2 doubling (that is, for years 201–220). Same as Fig. 4 but around the time of the 3rd CO2 doubling (that is, for years 201–220).

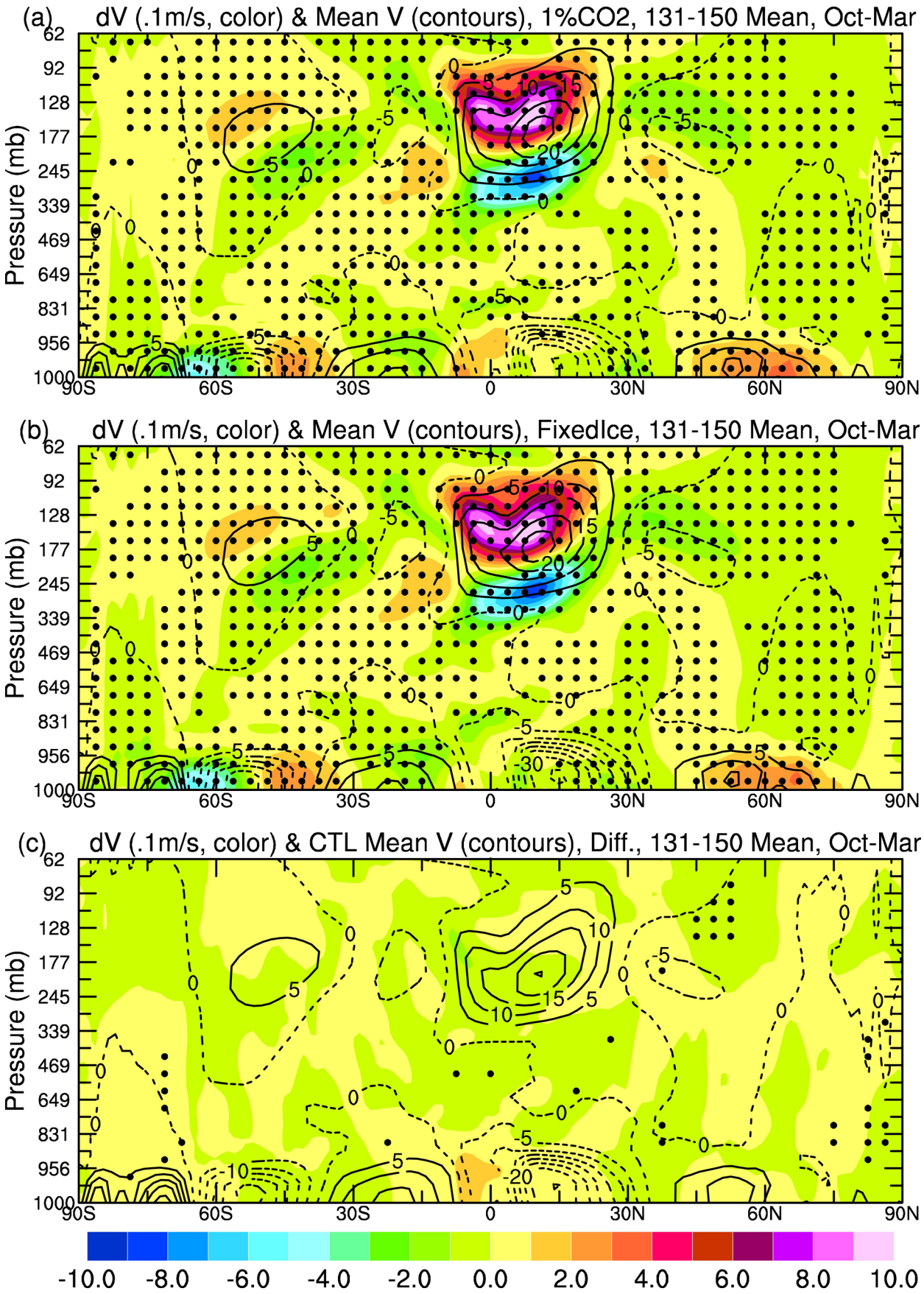

Extended Data Fig. 8 | See next page for caption.

Extended Data Fig. 8 | CESM1-simulated climatology (contours) and changes (color) in October-March zonal-mean V wind around the 2nd CO2 doubling (that is, for years 131–150). CESM1-simualted climatology (contours, in 0.1 m/s) and changes (color, in 0.1 m/s, relative the control-run climatology) averaged over years 131–150 of October-March zonal-mean meridional wind from the (**a**) 1% CO2 run and (**b**) FixedIce run. Panel **c** is the panel **a** minus **b** difference. Significant wind changes in (**a**, **b**) or differences in (**c**) at the 5% level are marked by the black dots. The contours in (**c**) are for the control-run climatology of the meridional wind. The changes around the 1st CO2 doubling (for years 61–80) have similar patterns with smaller magnitudes.

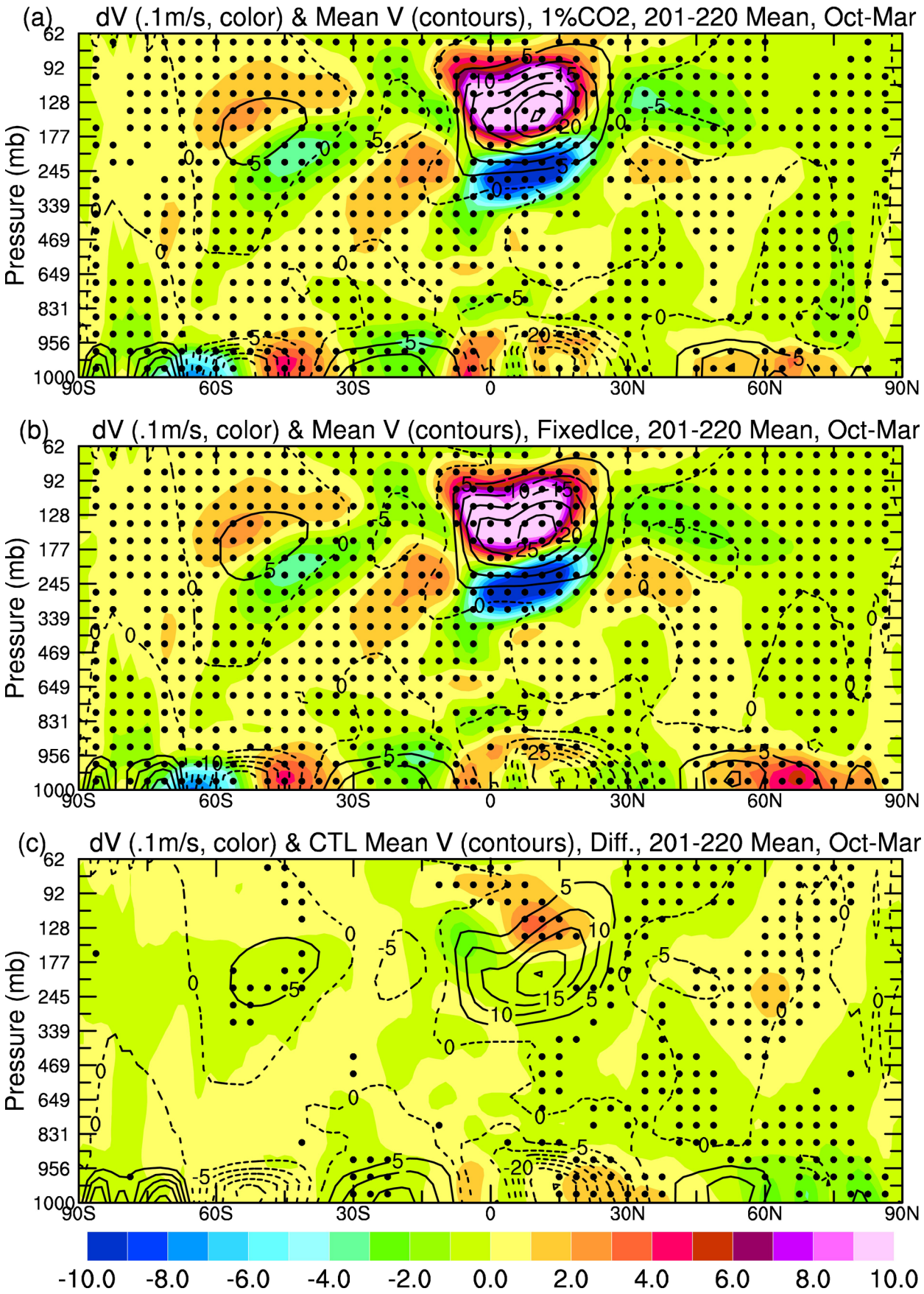

Extended Data Fig. 9 | CESM1-simulated climatology (contours) and changes (color) in October-March zonal-mean V wind around the 3rd CO2 doubling (that is, for years 201–220). Same as Extended Data Fig. 8, but for changes around the time of the 3rd CO2 doubling (that is, for years 201–220).

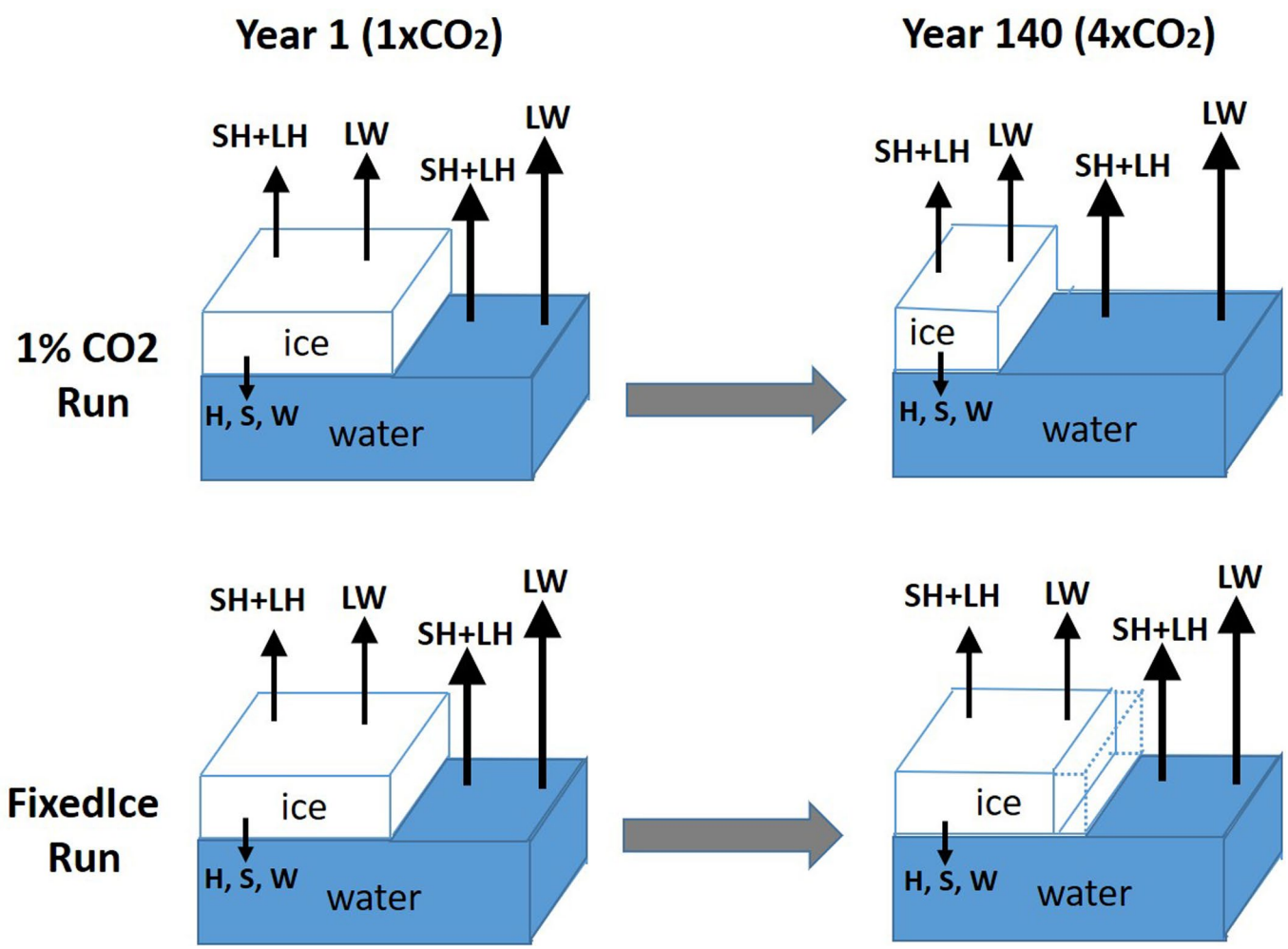

Extended Data Fig. 10 | Schematic diagram showing how the surface fluxes are applied in the standard 1%CO_2 run (top) and the FixedIce run (bottom) over Arctic sea-ice covered areas. Schematic diagram showing how the surface fluxes are applied in the standard 1%CO_2 run (top) and the FixedIce run (bottom) over Arctic sea-ice covered areas. In the FixedIce run (with the same 1%-per-year increase in atmospheric CO_2), sea-ice loss (outlined by the dashed lines in the lower-right panel) is small, and the fluxes from the ice model are applied to the same ice fraction as in year 1 (that is, they are extended to the volume outlined by the dashed lines in the lower-right panel), and the atmosphere and ocean components only see a fixed ice cover (with seasonal cycle). However, the ice model still dynamically calculates the ice fraction and the fluxes over sea ice. The ice model does not see this artificial ice fraction change but it feels the changed surface fluxes and near-surface states resulting from this change, and this leads to much slower ice melting and greatly reduced Arctic amplification in the FixedIce run than in the standard 1%CO_2 run. The main ice-atmosphere and water-atmosphere fluxes include sensible (SH) and latent (LH) heat fluxes, longwave (LW) and shortwave (not shown) radiative fluxes, and wind stress fluxes (not shown). The ice-ocean fluxes include heat (H), salt (S), freshwater (W), and wind stress (not shown) fluxes.

Supplementary Information for

Little Influence of Arctic Amplification on Midlatitude Climate

Aiguo Dai and Mirong Song

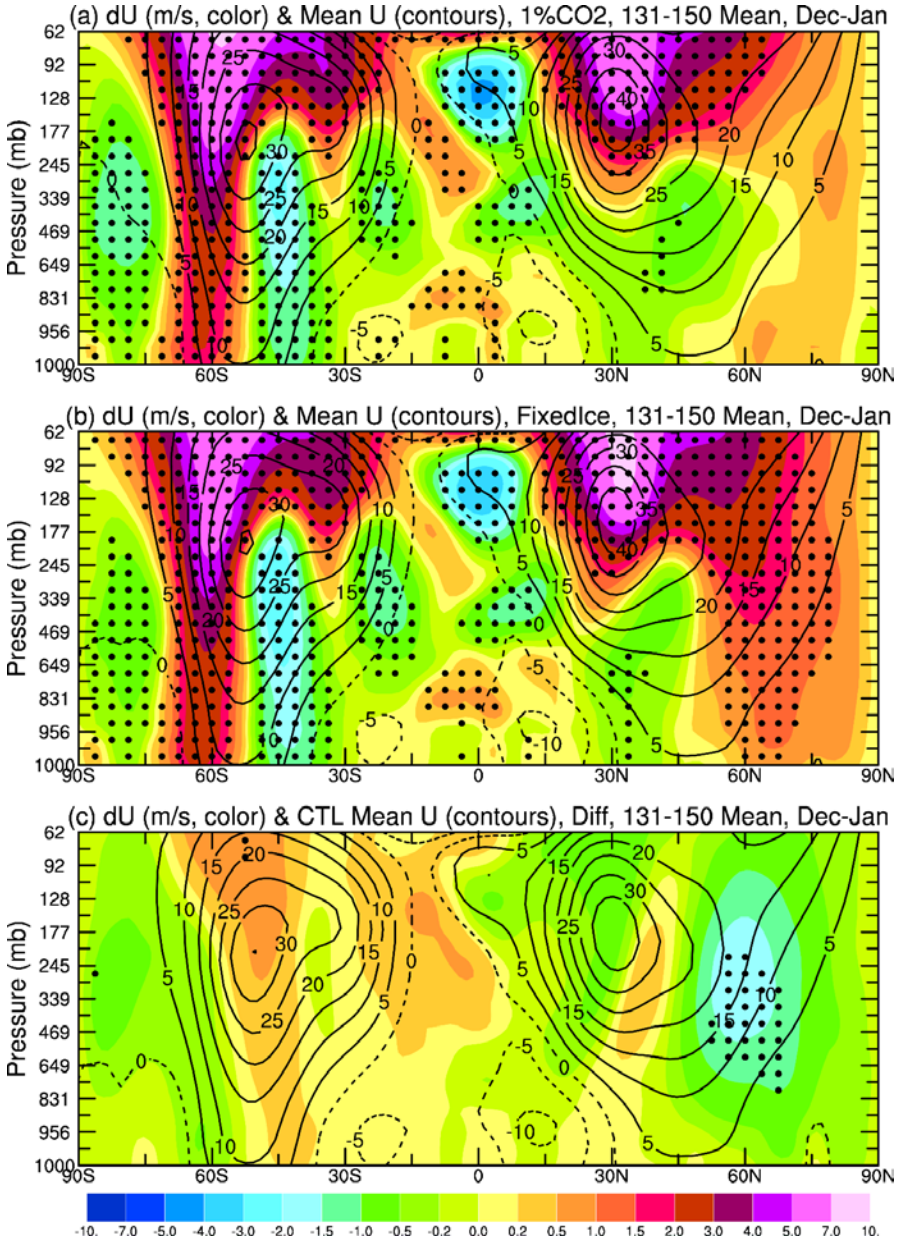

Figure S1. Same as Fig. 4 but for December-January averages.

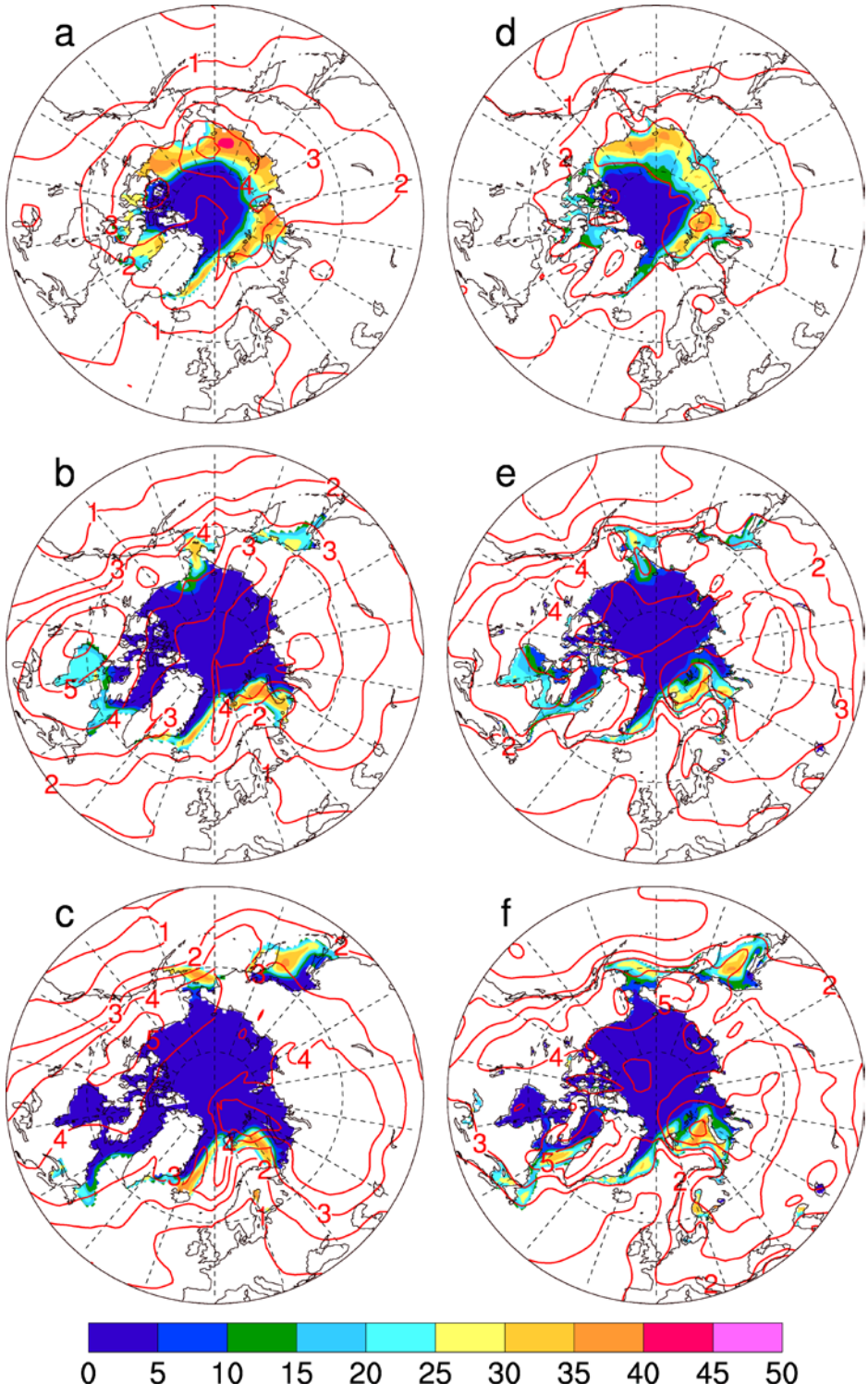

Figure S2. Standard deviations of the monthly sea-ice concentration (SIC, color shading, in %) and surface air temperature (red contours, in ºC) from CESM1-BGC all-forcing historical (for 1979-2005) and RCP8.5 (for 2006-2016) simulations (left column) and ERA-Interim (right column) during 1979-2016 for October (top), December (middle) and February (bottom).

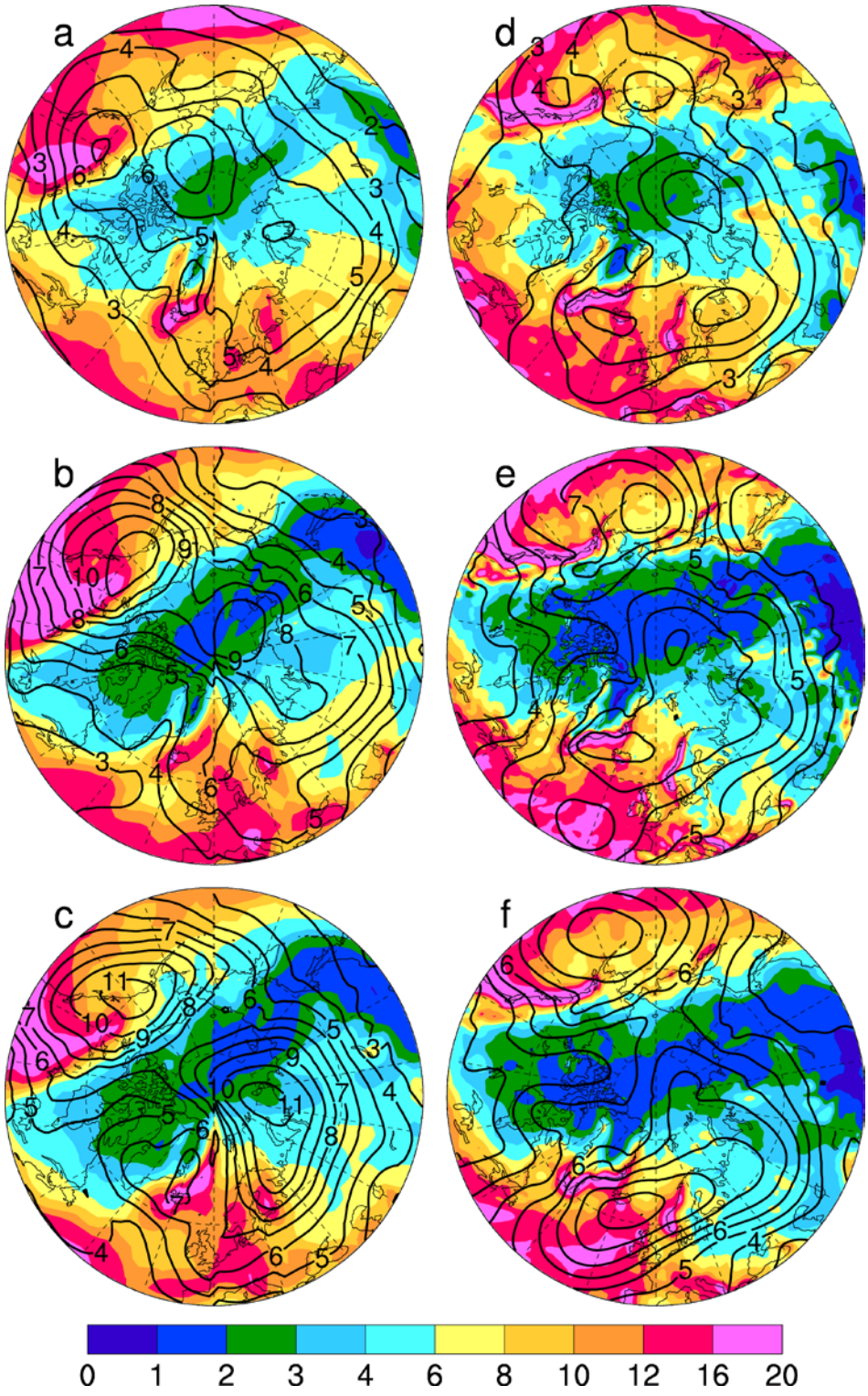

Figure S3. Standard deviations of the monthly precipitation (color shading, in 0.1mm/day) and sea-level pressure (contours, in hPa) from CESM1-BGC all-forcing historical (for 1979-2005) and RCP8.5 (for 2006-2016) simulations (left column) and ERA-Interim (right column) during 1979-2016 for October (top), December (middle) and February (bottom).

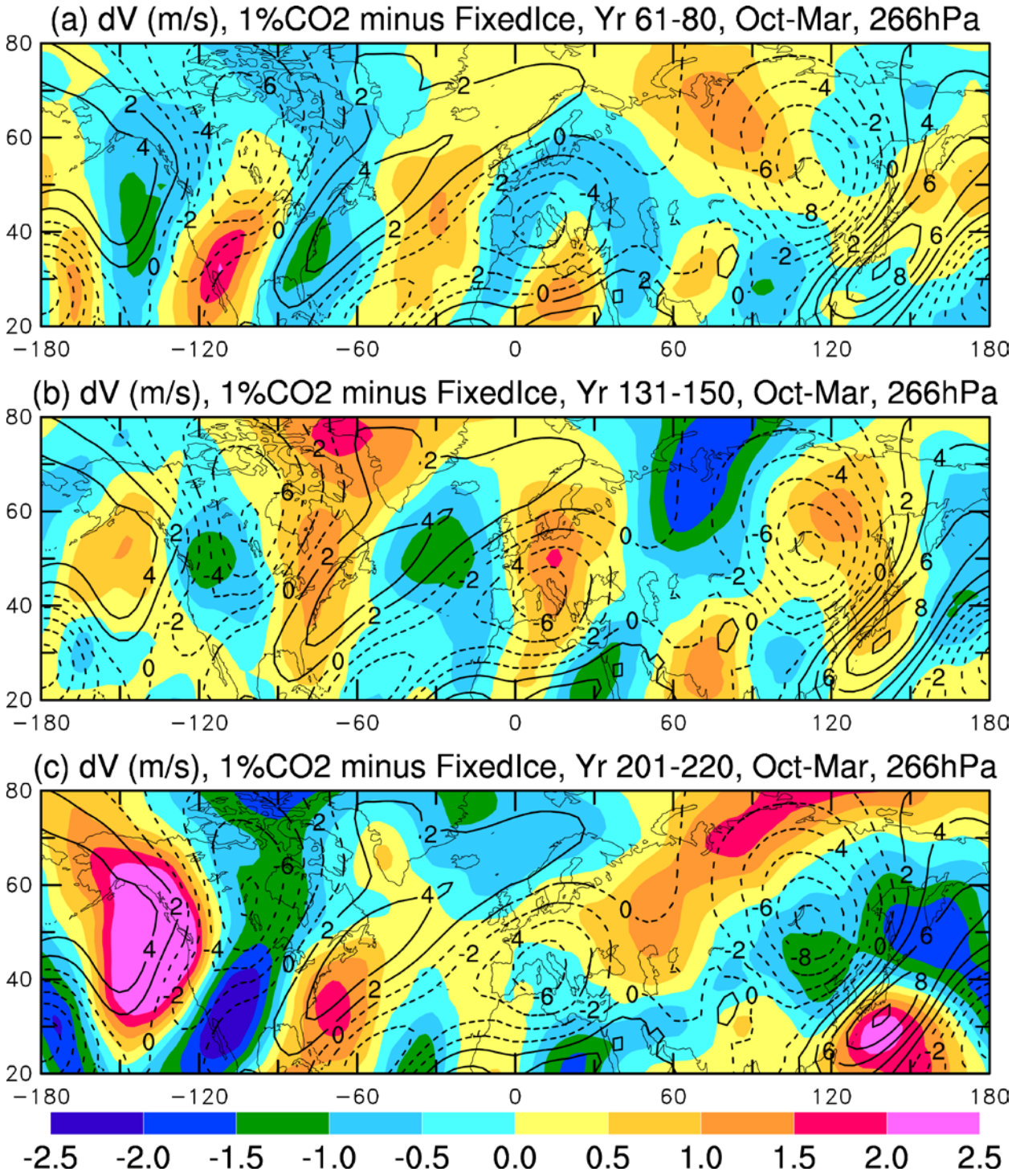

Figure S4. Spatial distribution of the 1% CO2 minus FixedIce difference (colour, in m s^{-1}) in October–March mean V at a level around 266 hPa averaged over years (a) 61-80, (b) 131–150, and (c) 201-220. The contours are the mean V (in m s^{-1}) from the control run.

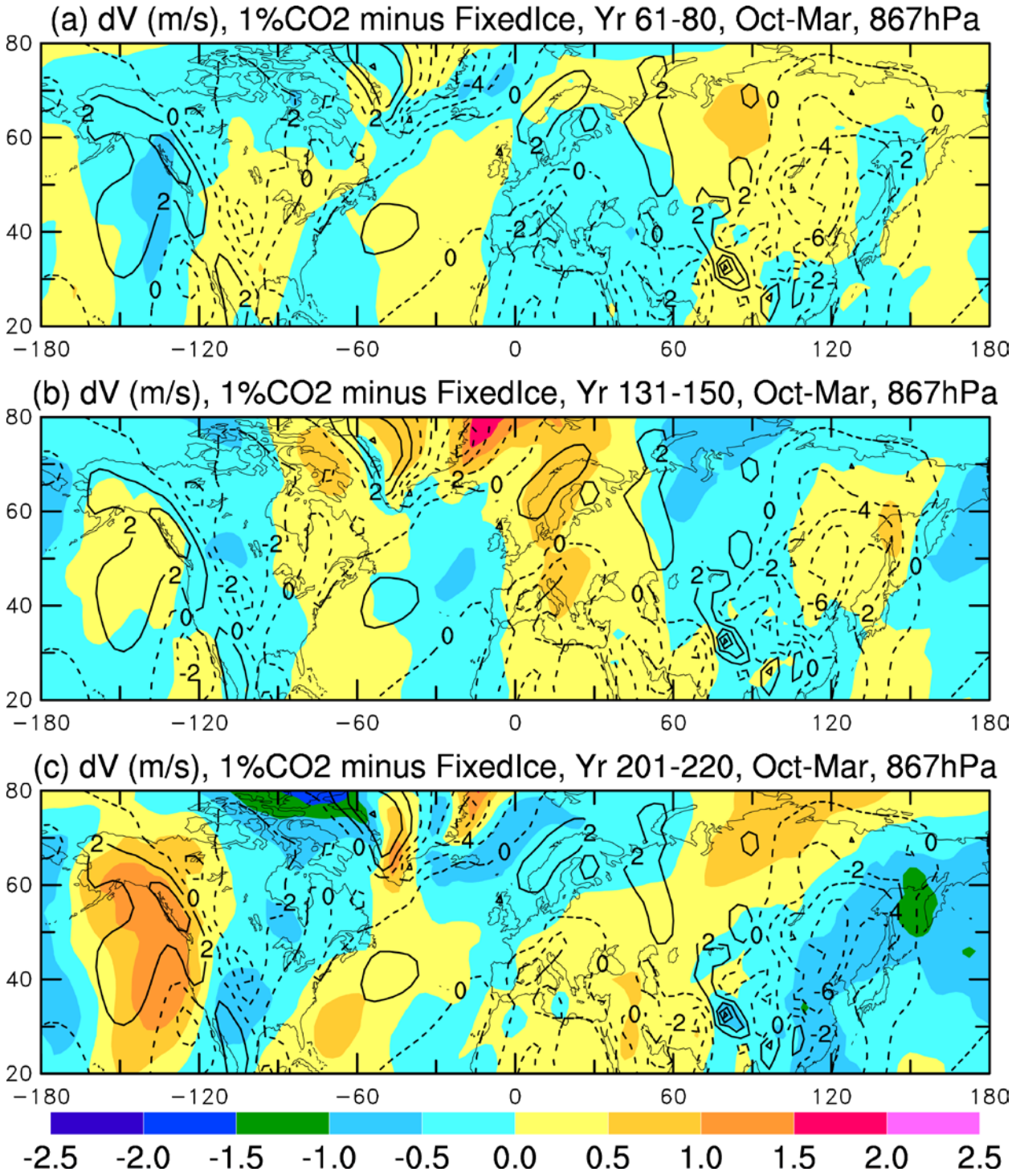

Figure S5. Spatial distribution of the 1% CO2 minus FixedIce difference (colour, in m s^{-1}) in October–March mean V at a level around 867 hPa averaged over years (a) 61-80, (b) 131–150, and (c) 201-220. The contours are the mean V (in m s^{-1}) from the control run.